

Caffeine enhances antitumor T-cell activity by suppressing kynurenine pathway in colorectal cancer

Received: 19 October 2024

Accepted: 5 June 2025

Published online: 01 July 2025



Yuechen Liu^{1,2,5}, Zhengyu Liu^{1,2,5}, Yating Hu^{1,2,5}, Yunyan Ling^{3,5}, Shunjie Qing^{1,2}, Yang Liu³, Yizhi Zhan⁴, Zhiyong Shen^{1,2}✉, Yuan Fang³✉ & Haijun Deng^{1,2}✉

Colorectal cancer (CRC) is a leading global health issue, ranking third in incidence and second in cancer mortality. Immunotherapy, effective mainly in mismatch repair-deficient CRC, may benefit from dietary interventions. This study investigates caffeine's potential to boost programmed death-1 (PD-1) immunotherapy efficacy in CRC, revealing that caffeine significantly reduces tumor growth, extends survival, and enhances CD8⁺ T cell activity in CRC by suppressing kynurenine pathway. Mechanistically, caffeine decreases kynurenine via the Krüppel-like factor 4 (KLF4)-Collagen type XII alpha 1 (COL12A1)-Mitogen-Activated Protein Kinase (MAPK)-Indoleamine 2,3-dioxygenase 1 (IDO1) axis, mitigating CD8⁺ T cell exhaustion. Combining caffeine with PD-1 therapy further prolongs survival, highlighting the value of integrating nutritional strategies into cancer treatment to improve outcomes and broaden therapeutic options. Here, we show caffeine can enhance PD-1 immunotherapy in CRC by suppressing kynurenine pathway, suggesting its potential as an adjunctive dietary therapy.

Colorectal cancer (CRC) ranks as the third most common cancer worldwide and is the second leading cause of cancer-related deaths^{1,2}. Although immunotherapy represents a significant breakthrough in cancer treatment, its benefits are not yet universal among CRC patients. At present, only CRC patients with mismatch repair deficiency or high microsatellite instability (MSI-H) benefit from immune checkpoint inhibitors^{3,4}. Importantly, only 15% of CRC cases are MSI-H, and this percentage decreases to 4–5% in advanced stages⁵. Therefore, it is crucial to expand the scope of CRC immunotherapy to benefit a broader patient population or combine other treatments to boost immunotherapy.

Tumor development and progression are strongly influenced by dietary habits. Dietary interventions can aid tumor treatment by limiting tumor nutrition, boosting drug efficacy, and enhancing the

immune microenvironment^{6–8}. Research indicates that diets rich in serine and glycine may accelerate colorectal cancer progression through the induction of KRAS and TP53 mutations⁹. Diets high in methionine may foster colorectal cancer growth by activating the immune microenvironment via m⁶A methylation in tumor cells¹⁰. Diets containing mannose can impede colorectal cancer metastasis by inhibiting fructose metabolism¹¹. Thus, dietary interventions are vital in managing colorectal cancer and could potentially enhance the effectiveness of immunotherapy. The role of dietary components in influencing immunotherapy for colorectal cancer remains to be further investigated.

Coffee is a staple beverage worldwide. Numerous studies suggest that coffee may help prevent colorectal cancer, offering potential

¹Department of General Surgery, Nanfang Hospital, Southern Medical University, Guangzhou, Guangdong Province, China. ²Department of General Surgery & Guangdong Provincial Key Laboratory of Precision Medicine for Gastrointestinal Tumor, Nanfang Hospital, Southern Medical University, Guangzhou, Guangdong Province, China. ³Department of Radiation Oncology, Nanfang Hospital, Southern Medical University, Guangzhou, Guangdong Province, China. ⁴Department of Pathology, Nanfang Hospital, Southern Medical University, Guangzhou, Guangdong Province, China. ⁵These authors contributed equally: Yuechen Liu, Zhengyu Liu, Yating Hu, Yunyan Ling. ✉e-mail: szy2728@163.com; fangyuan1313@163.com; navyd999@163.com

health benefits^{12–14}. Although a cup of coffee contains hundreds of compounds, the levels of which can vary due to different production and preparation processes, caffeine is the primary component across various coffee types. Caffeine, a purine alkaloid, has been reported to inhibit intestinal inflammation and regulate the gut microbiome, potentially lowering the risk of colorectal cancer^{15,16}. Additionally, caffeine inhibits the adenosine A2A receptor, reducing adenosine's immunosuppressive effects and enhancing macrophages' phagocytic and antitumor activities¹⁷. Research combining caffeine with anti-PD-1 therapy in melanoma has shown that this treatment can effectively inhibit melanoma growth and significantly increase CD4⁺ and CD8⁺ T lymphocyte infiltration¹⁸. However, what effect caffeine has on colorectal cancer and the specific mechanism remains unknown.

COL12A1 (Collagen type XII alpha 1), a collagen protein involved in the extracellular matrix, has been implicated in various cancers, including CRC, where its expression correlates with poor prognosis and reduced immune cell infiltration^{19–22}. Additionally, the IDO1 (Indoleamine 2,3-dioxygenase 1) enzyme and its downstream product, kynurenine, play a crucial role in immune suppression, particularly in T cell exhaustion and the development of an immunosuppressive tumor microenvironment^{23–25}. However, whether the COL12A1/IDO1/Kynurenine pathway is involved in the effects of caffeine on colorectal cancer and the specific mechanisms remain unknown.

In this work, we report that caffeine inhibits colorectal cancer progression and improves survival in various mouse models. Its anti-tumor effects are linked to the alleviation of CD8⁺ T-cell exhaustion. Specifically, caffeine may activate CD8⁺ T cells by downregulating COL12A1 expression in tumor cells, consequently reducing kynurenine production through the MAPK-IDO1 axis. Additionally, caffeine exhibits an immune-sensitizing effect that enhances the efficacy of PD-1 antibody immunotherapy in colorectal cancer. Furthermore, COL12A1 could serve as a biomarker for immunotherapy nonresponse in cancer patients. By integration of dietary components, specifically caffeine, with cutting-edge immunotherapeutic strategies, our research not only advances the understanding of CRC immunology but also highlights dietary interventions as a potent therapeutic modality in cancer treatment.

Results

Caffeine inhibits colorectal cancer progression and enhances survival

To assess caffeine's impact on colorectal cancer, we analyzed dietary habits from the UK Biobank database, revealing that higher caffeine intake correlates with improved prognosis and survival (Fig. 1a). We then used the APC^{min/+} mice model with spontaneous tumors, treating them with 0.1% caffeine water. The results showed significant reductions in adenoma count and tumor weight in the caffeine-treated group compared to controls (Fig. 1b). We established subcutaneous and cecal orthotopic tumor models, treating them with either normal water or 0.1% caffeine water. In the caffeine-treated group, mice showed slower tumor growth, with reduced tumor volumes and tumor weights compared to controls. And survival was significantly prolonged in the caffeine-treated mice (Fig. 1c–h). Additionally, caffeine treatment did not significantly affect body weight, liver and spleen weights, or serum levels of ALT, AST, BUN, and CREA, indicating its safety in APC^{min/+} and BALB/c mice (Supplementary Fig. 1a–f). These results suggest that caffeine can inhibit colorectal cancer progression and enhance survival.

Next, we established subcutaneous tumor models in both immunocompetent and immunodeficient mice, treating them with either normal or 0.1% caffeine water. Results indicated that caffeine significantly inhibited tumor growth in immunocompetent mice, but did not affect tumor growth in nude mice (Fig. 1i, j, Supplementary Fig. 1g, h). This suggests that the effect of caffeine in inhibiting colorectal cancer progression is related to the immune microenvironment.

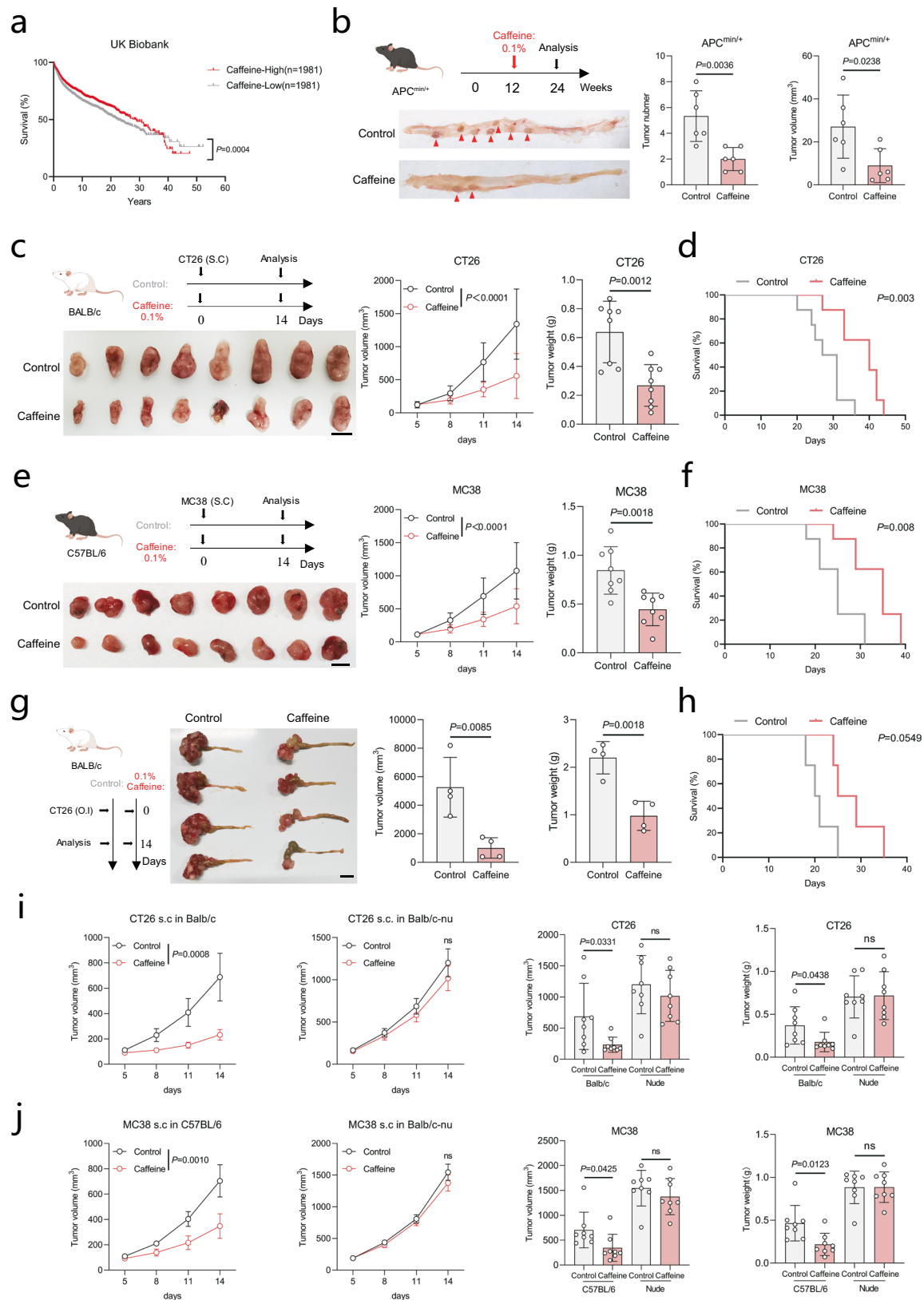
The anti-tumor effect of caffeine depends on CD8⁺ T-cell function

To assess the impact of caffeine on the tumor immune micro-environment, we analyzed immune cell expression and proportions using flow cytometry in tumors from immunocompetent subcutaneous, orthotopic, and spontaneous APC^{min/+} mouse models. Analysis revealed a significant increase in CD8⁺ T cells and a reduction in exhaustion markers (PD-1, LAG3) in the caffeine-treated group (Fig. 2a, b, Supplementary Fig. 2a–c). No significant changes were observed in other immune cells, including CD4⁺ T cells, B cells, neutrophils, and macrophages, between the caffeine-treated and control groups (Fig. 2c, d, Supplementary Fig. 2d, e). Immunohistochemistry and qPCR analyses of tumor tissues showed an increase in CD8⁺ T cells and cytotoxic markers (GZMB, IFNG), and a decrease in exhaustion markers (PD-1, LAG3) in the caffeine-treated group (Fig. 2e, f, Supplementary Fig. 2f–k). To elucidate the link between caffeine's anti-tumor effect and CD8⁺ T cells, we established cecal orthotopic and subcutaneous tumor models treated with caffeine and anti-CD8 monoclonal antibody. Results indicated that depleting CD8⁺ T cells with anti-CD8 monoclonal antibody significantly reversed caffeine's anti-tumor effect on colorectal cancer (Fig. 2g–j, Supplementary Fig. 2l–o). These findings indicate that the anti-tumor effect of caffeine depends on CD8⁺ T-cell functional exhaustion.

COL12A1 is a crucial molecule in the anti-tumor effects of caffeine

To explore how caffeine activates CD8⁺ T cells, we conducted co-culture experiments using Jurkat cells and HCT116 cells treated with caffeine. Results of flow cytometry and qPCR indicated that caffeine affected Jurkat cells exhaustion only in the presence of tumor cells (Fig. 3a–d, Supplementary Fig. 3a). Additionally, we treated extracted mouse CD8⁺ T cells directly with caffeine or co-culture with MC38 cells and assessed CD8⁺ T cell activation via flow cytometry and qPCR. Results indicated that direct caffeine treatment did not alter CD8⁺ T cell activation (Supplementary Fig. 3b–f). This suggests that caffeine activates CD8⁺ T cells by affecting tumor cells. Next, we performed transcriptomic sequencing on caffeine-treated and untreated HCT116 cells. The results showed that caffeine primarily influences tryptophan metabolism (Fig. 3e, f, Supplementary Fig. 3g). We screened for genes downregulated in caffeine-treated cells, highly expressed in tumor tissues in the TCGA database, and correlated with prognosis. Subsequently, we identified *COL12A1* as a target gene (Fig. 3g).

COL12A1 is a member of the fibrillar collagen family, a predominant constituent of the extracellular matrix to maintain tissue structure and function. COL12A1 is upregulated in various cancers, including gastric, colorectal, and breast cancer, possibly affecting the migratory and invasive capabilities of tumor cells^{19,21,22}. Further research has demonstrated that COL12A1 positively correlates with the abundance of M2 macrophage infiltration in tumors and exhibits significant expression differences between responding and non-responding patients undergoing immunotherapy²⁰. However, in colorectal cancer, whether COL12A1 is a critical target for caffeine's anti-tumor effect and how it influences T cell exhaustion is currently unknown. Further bioinformatics analysis indicated that in colorectal cancer, COL12A1 significantly correlates with immune-related markers, and CD8⁺ T cell populations (Supplementary Fig. 3h–j). Using human colorectal cancer tumor tissues and public databases, we found that COL12A1 was upregulated in tumors (Fig. 3h, i, Supplementary Fig. 3k). Further IHC results and analysis of human colorectal cancer tissue microarrays showed that high COL12A1 expression in colorectal cancer tissues correlates with reduced CD8⁺ T cell levels and poor prognosis. In addition to its prognostic significance, COL12A1 was strongly associated with various malignant clinicopathological features and an increased mortality risk in CRC patients (Fig. 3j–m, Supplementary Fig. 3l, m). The above results suggest that COL12A1 may be a key molecule in the anti-tumor effect of caffeine.



Caffeine activates CD8⁺ T cells by KLF4/COL12A1 axis in CRC cells

To determine if caffeine activates CD8⁺ T cells via COL12A1, we treated colorectal cancer cells with varying caffeine concentrations. We observed a dose-dependent downregulation of COL12A1 in CRC cells by caffeine (Fig. 4a, b). We then constructed CRC cells with different

expression of COL12A1 (Supplementary Fig. 4a–d). Next, we treated the COL12A1-overexpression CRC cells with caffeine to assess its effects on expression levels. Results indicated that caffeine significantly downregulated COL12A1 expression in tumor cells (Fig. 4c, d). Next, we used a subcutaneous tumor mice with overexpressed-COL12A1 MC38 cells and treated with caffeine. Results

Fig. 1 | Caffeine inhibits colorectal cancer progression and enhances survival.

a Survival analysis using Kaplan-Meier method from the UK Biobank dataset comparing high and low caffeine intake groups in colorectal cancer patients ($n = 1981$). **b** Schematic depicting the treatment of caffeine (0.1% w/v, daily) in APC^{min/+} mice. Representative images of intestinal tumor (red arrows) and quantification of tumor number and tumor volume ($n = 6$ per group). **c** Schematic depicting the treatment of caffeine (0.1% w/v, daily) in subcutaneous CT26 tumor-bearing BALB/c mice. Representative images of tumor from control and caffeine-treated groups ($n = 8$ per group). Scale bars, 1 cm. Quantification of the tumor growth curve and tumor weight. **d** Kaplan-Meier survival curves of CT26 tumor-bearing BALB/c mice treated with caffeine or control ($n = 8$ per group). **e** Schematic depicting the treatment of caffeine (0.1% w/v, daily) in subcutaneous MC38 tumor-bearing C57BL/6 mice. Representative images of tumor from control and caffeine-treated groups ($n = 8$ per group). Scale bars, 1 cm. Quantification of the tumor growth curve and tumor weight. **f** Kaplan-Meier survival curves of MC38 tumor-

bearing C57BL/6 mice treated with caffeine or control ($n = 8$ per group). **g** Schematic depicting the treatment of caffeine (0.1% w/v, daily) in orthotopic CT26 tumor-bearing BALB/c mice. Representative images of tumor from control and caffeine-treated groups ($n = 4$ per group). Scale bars, 1 cm. Quantification of the tumor volume and tumor weight. **h** Kaplan-Meier survival curves of orthotopic CT26 tumor-bearing BALB/c mice treated with caffeine or control ($n = 4$ per group). **i** Tumor growth curves and tumor weights of subcutaneous CT26 tumor-bearing BALB/c and BALB/c-nu mice treated with caffeine (0.1% w/v, daily) or control ($n = 8$ per group). **j** Tumor growth curves and tumor weights of subcutaneous MC38 tumor-bearing C57BL/6 mice and BALB/c-nu mice treated with caffeine (0.1% w/v, daily) or control ($n = 8$ per group). s.c., subcutaneous inject. o.i., orthotopic inject. Data error bars are mean \pm SD. The statistical analysis of tumor growth curve is Two-way ANOVA, the survival curve is Log-rank test, the others are Student's two-tailed unpaired t-test. The images of mice elements were drawn by Figdraw. Source data are provided as a Source Data file.

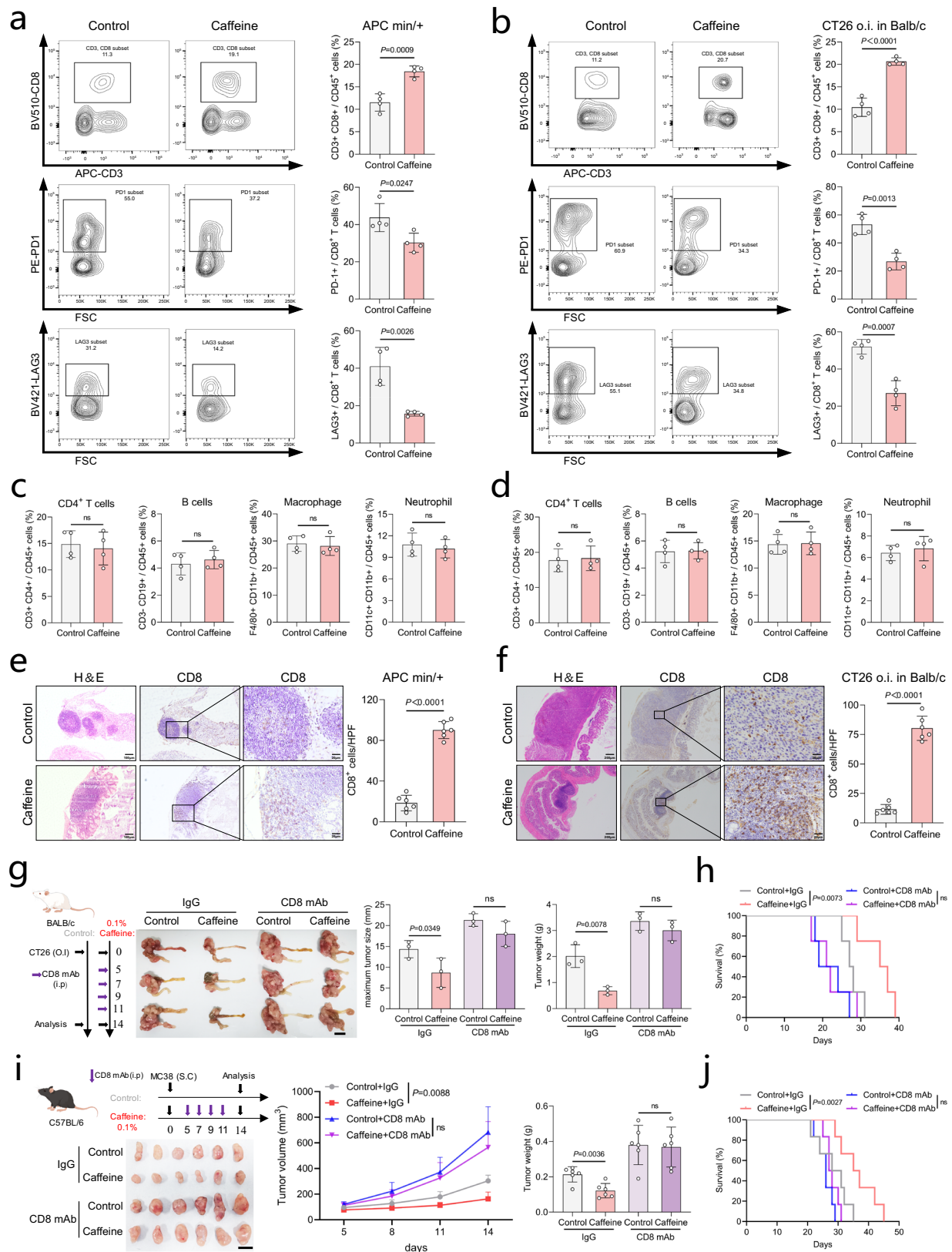
demonstrated that COL12A1 overexpression significantly reversed caffeine's anti-tumor effect and suppressed CD8⁺ T cell infiltration and cytotoxicity in tumors (Fig. 4e–g, Supplementary Fig. 4e, f). Furthermore, we established a subcutaneous tumor mice model with COL12A1 knockdown MC38 cells and treated with anti-CD8 monoclonal antibody. In the COL12A1 knockdown group, subcutaneous tumor growth slowed, tumor weight decreased, and CD8⁺ T cell infiltration increased. Depletion of CD8⁺ T cells significantly reversed the anti-tumor effect of COL12A1 knockdown (Fig. 4h–j, Supplementary Fig. 4g, h). These findings indicate that caffeine inhibits colorectal cancer by downregulating COL12A1 to activate CD8⁺ T cells. Furthermore, we conducted in vitro co-culture experiments and found that caffeine significantly enhanced the cytotoxic and proliferative capacities of CD8⁺ T cells, while COL12A1 overexpression reversed this activation (Fig. 4k, Supplementary Fig. 4i). The above results suggest that caffeine may activate CD8⁺ T cells by downregulating COL12A1 expression in tumor cells.

Next, we conducted a preliminary investigation into the direct mechanism by which caffeine regulates COL12A1 expression. Using the hTF-target and JASPAR databases (relative profile score threshold >99%, score >10, multiple binding sites), we predicted upstream transcription factors of COL12A1 and identified 15 with differential expression. Subsequently, we treated CRC cells with caffeine and assessed mRNA expression of these transcription factors using qPCR, revealing that only KLF4 was consistently upregulated across all cell lines (Supplementary Fig. 4j). Krüppel-like factor 4 (KLF4), a key transcription factor, regulates multiple processes, including DNA damage response, inflammation, apoptosis, and stem cell reprogramming, playing a critical role in the progression of aggressive cancers^{26–28}. In tumors, KLF4 promotes CD8⁺ T-cell differentiation and upregulates AP-1 family factors, such as c-Jun, conferring transient effector characteristics to tumor-specific CD8⁺ T cells^{29,30}. Pearson correlation analysis further showed a positive correlation between KLF4 and COL12A1 expression (Supplementary Fig. 4k). Additionally, ChIP assays confirmed that anti-KLF4 significantly enhanced COL12A1 enrichment (Supplementary Fig. 4l). Furthermore, western blot and qRT-PCR analyses demonstrated a significant reduction in COL12A1 expression following KLF4 overexpression in HCT116 cells (Supplementary Fig. 4m, n). Using the JASPAR database, we identified potential binding sites between KLF4 and the 2000bp upstream region of the COL12A1 transcript. Dual-luciferase reporter assays confirmed that KLF4 overexpression significantly reduced the luciferase activity of COL12A1-WT, but no notable effect was observed with COL12A1-MUT1/3 (Supplementary Fig. 4o, p). These data suggest that KLF4 can directly bind to the COL12A1 promoter in binding site 2 and participate in COL12A1 transcription, acts as an upstream regulator of COL12A1. However, the precise mechanism by which caffeine modulates KLF4 expression remains to be elucidated.

Caffeine downregulates COL12A1 to reduce kynurenine

Previous literature indicates that tumor cells can domesticate immune cells in the microenvironment by secreting various metabolites, proteins, and cytokines, consequently mediating the functional dysfunction³¹. To investigate whether caffeine affects CD8⁺ T cells by altering protein secretion or metabolite production in tumor cells, we collected tumor-conditioned media (TCM) from caffeine-treated and untreated HCT116 cells. The TCM was filtered by molecular weight (distinguishing large proteins from small metabolites), boiled, and subsequently used to culture Jurkat cells. The results showed that the metabolome (<3 kDa) could influence markers expression, while the large protein fraction (>3 kDa) and boiling treatment did not affect, indicating that caffeine influences CD8⁺ T cells by affecting metabolite production in tumor cells (Supplementary Fig. 5a, b). We conducted metabolomic sequencing on supernatants from caffeine-treated and untreated tumor cells to identify which metabolites are involved in activating CD8⁺ T cells. Metabolomic analysis revealed that caffeine treatment primarily affects tryptophan metabolism, consistent with the previous transcriptomic sequencing (Fig. 5a, b). Additionally, caffeine treatment significantly increasing tryptophan and decreasing kynurenine levels (Fig. 5c–e, Supplementary Fig. 5d).

Tryptophan metabolism occurs via three pathways, predominantly through the kynurenine (Kyn) pathway, which metabolizes over 95% of tryptophan (Supplementary Fig. 5c). It has been reported that Kyn plays a crucial role in regulating tumor cells and reshaping the immune microenvironment^{32–34}. Kyn enhances tumor cell malignancy and affects immune cells like inhibiting T cell proliferation, promoting Treg cell differentiation, and recruiting macrophages, thus contributing to an immunosuppressive microenvironment and immunotherapy resistance^{25,35,36}. We then treated HCT116 cells with caffeine and performing ELISA to examine four other metabolites (3-hydrokynurenine, Kynurenic acid, Picolinic acid and Quinolinic acid) with differential results in the kynurenine pathway. However, these four metabolites did not yield consistent results like kynurenine (Supplementary Fig. 5e). Further ELISA tests revealed that caffeine significantly reduced Kyn levels in both tumor cells and supernatants with a concentration-dependent effect, while overexpression of COL12A1 could restore Kyn levels (Fig. 5f, g). These findings preliminarily suggest that caffeine's anti-tumor effect may derive from reducing Kyn production. Using ELISA assay, we found significantly higher Kyn levels in tumor tissues compared to normal tissues (Supplementary Fig. 5f). Next, we conducted a subcutaneous tumor mice model with CT26 cells, treated mice with caffeine and kynurenine or Indoximod (IDO pathway inhibitor). Results showed that tumor growth slowed in the caffeine treatment group, accelerated in the kynurenine supplement group, and returned to control group levels in caffeine+Kyn group, indicating that exogenous kynurenine reversed caffeine's anti-cancer effect. Tumor growth slowed in Kyn+Indoximod group (similar to Caffeine treatment group), suggesting that reducing kynurenine alone is



sufficient to inhibit tumors. Caffeine+Kyn+Indoximod group showed no significant difference from Kyn+Indoximod group, indicating that caffeine's anti-cancer effect primarily depends on reducing kynurenine production, with no notable additional effects. Related flow cytometry and immunohistochemistry staining results also support these findings. The above results suggested that caffeine's anti-cancer

mechanism primarily operates through the regulation of kynurenine production. Kyn is involved in the caffeine-mediated anti-cancer effects (Fig. 5h–j, Supplementary Fig. 5g, h). We further developed a subcutaneous tumor mice model with COL12A1-overexpressing CT26 cells, treated mice with caffeine or Indoximod. Results showed that inhibiting Kyn production restored the tumor-promoting effect of

Fig. 2 | The anti-tumor effect of caffeine depends on CD8⁺ T-cell function. Flow cytometry analysis of CD8⁺ T cells and exhaustion markers (PD-1, LAG3) in **a** spontaneous tumor in APC^{min/+} mice and **b** orthotopic CT26 tumor in BALB/c mice treated with caffeine (0.1% w/v, daily) or control ($n = 4$ per group). Quantification of immune cell populations (CD4⁺ T cells, B cells, macrophages, and neutrophils) in **c** spontaneous tumor in APC^{min/+} mice and **d** orthotopic CT26 tumor in BALB/c mice treated with caffeine or control ($n = 4$ per group). Immunohistochemistry staining and quantification of CD8⁺ T cells in **e** spontaneous tumor in APC^{min/+} mice and **f** orthotopic CT26 tumor in BALB/c mice treated with caffeine or control ($n = 6$ per group). Scale bars, 200 μ m, 100 μ m, 20 μ m. **g** Schematic depicting the treatment of caffeine (0.1% w/v, daily) or anti-CD8 monoclonal antibody (CD8 mAb, 200 μ g/mouse, ip. twice weekly) in orthotopic CT26 tumor-bearing BALB/c mice. Representative images of tumor from control or caffeine-treated and CD8 mAb treatment groups ($n = 3$ per group). Scale bars, 1 cm. Quantification of the maximum tumor

size and tumor weight. **h** Kaplan-Meier survival curves of orthotopic CT26 tumor-bearing BALB/c mice treated with caffeine or control and CD8 mAb ($n = 4$ per group). **i** Schematic depicting the treatment of caffeine (0.1% w/v, daily) and CD8 mAb (200 μ g/mouse, ip. twice weekly) in subcutaneous MC38 tumor-bearing C57BL/6 mice. Representative images of tumor from control or caffeine-treated and CD8 mAb treatment groups ($n = 6$ per group). Scale bars, 1 cm. Quantification of the tumor growth curve and tumor weight. **j** Kaplan-Meier survival curves of subcutaneous MC38 tumor-bearing C57BL/6 mice treated with caffeine or control and CD8 mAb ($n = 6$ per group). s.c., subcutaneous inject. o.i., orthotopic inject. Data error bars are mean \pm SD. The statistical analysis of tumor growth curve is Two-way ANOVA, the survival curve is Log-rank test, the others are Student's two-tailed unpaired t-test. The images of mice elements were drawn by Figdraw. Source data are provided as a Source Data file.

COL12A1, with consistent changes in CD8⁺ T cell infiltration and effector markers (Fig. 5k–m, Supplementary Fig. 5i, j). Next, we co-cultured mouse spleen cells with COL12A1-overexpressing CT26 cells treated with caffeine, Kyn or Indoximod, measuring cytotoxic exhaustion markers and CD8⁺ T cell proliferation. Results indicated that COL12A1 overexpression or Kyn supplementation significantly inhibited CD8⁺ T cell activation, while Indoximod significantly enhanced it (Fig. 5n, Supplementary Fig. 5k). The above results indicate that caffeine may promote CD8⁺ T cell activation by downregulating COL12A1, affecting tryptophan metabolism, and reducing kynurenine production.

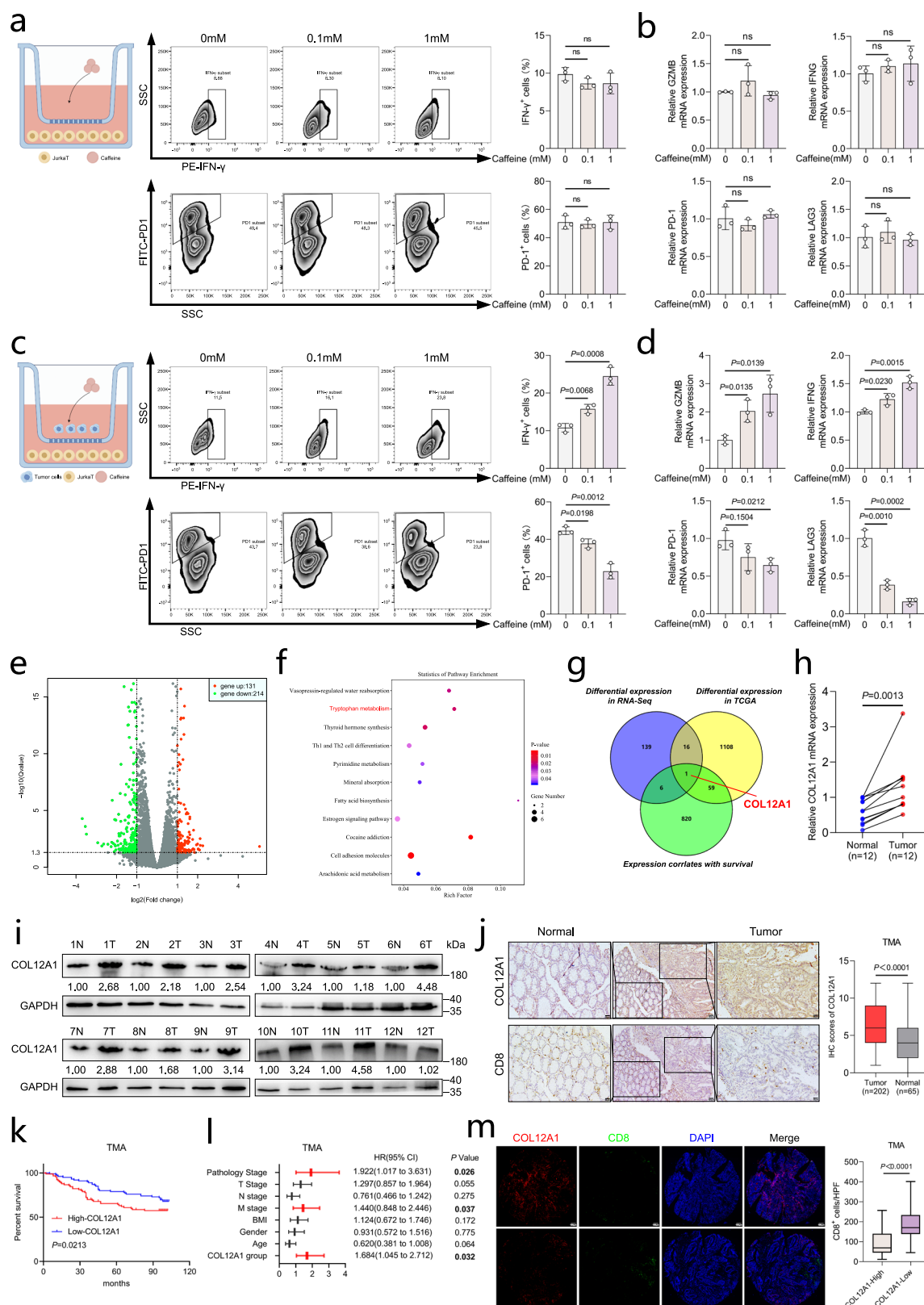
COL12A1 regulates Kyn production via MAPK-IDO1 axis

Given the changes of the metabolite concentration of CRC cells with caffeine treatment, we further explored the metabolic phenotype of CRC cells. We measured mitochondrial function and aerobic glycolysis in CRC cells to evaluate the effect of caffeine with SeaHorse. The results showed that caffeine treatment significantly reduced the extracellular acidification rate (ECAR) while markedly increasing the oxygen consumption rate (OCR) in HCT116 cells (Supplementary Fig. 6a, b). The results indicated that caffeine could inhibit the aerobic glycolysis of CRC. Previous studies have also shown that KLF4 upregulation is generally associated with glycolysis suppression^{37,38}, which aligns with our prior findings that caffeine treatment upregulated KLF4 while reducing COL12A1 expression. However, the specific mechanisms by which caffeine regulates KLF4 and glycolysis require further investigation.

We further investigate how COL12A1 affects kynurenine production. It has reported that COL12A1 is a type of collagen and a secreted protein. Previous research about COL12A1 have not yet investigated its ability to influence tumor cells through an autocrine manner. We consequently exogenously added COL12A1 protein to the tumor cell culture medium and subsequently measured the levels of Kyn in the tumor supernatant. We found that this did not affect the secretion of Kyn by the tumor cells (Supplementary Fig. 6c). Therefore, we speculate that COL12A1 mainly does not influence immune cells through the secreted protein pathway. This suggests that COL12A1 may influence the production of Kyn through the signaling axis within the tumor cells rather than an autocrine manner.

Since kynurenine is primarily produced through tryptophan metabolism, we analyzed the expression of key enzymes (IDO1, IDO2, TDO2) of tryptophan metabolism in colorectal cancer cells with varying COL12A1 levels. Results indicated that COL12A1 significantly and consistently affect IDO1 expression (not IDO2 or TDO2) in all colorectal cancer cells (Fig. 6a–c). IDO1 is an essential immune-regulatory enzyme, by catalyzing the degradation of tryptophan to produce kynurenine, inhibits T cell proliferation and promotes the generation of regulatory T cells^{23,24,39}. Inhibiting IDO1 activity can restore T cell function, enhance anti-tumor immune responses, and improve the therapeutic effects of immune checkpoint inhibitors (such as PD-1/PD-

L1 inhibitors)^{40,41}. Through bioinformatics analysis, we found that IDO1 was highly expressed in tumor tissues and correlated with COL12A1 expression in CRC (Supplementary Fig. 6e, d). In addition, both IDO1 and COL12A1 were associated with caffeine metabolism and tryptophan metabolism pathway (Supplementary Fig. 6f, g), indicating that IDO1 may be involved in the regulatory mechanism of caffeine and COL12A1. Additionally, Indoximod can effectively reverse the tumor-promoting and immunosuppressive effects of COL12A1 overexpression. Based on our existing experimental results, we hypothesize that caffeine influences IDO1 expression by downregulating COL12A1, thereby modulating kynurenine production. We further investigated how COL12A1 specifically regulates the expression of IDO1. We performed transcriptomic sequencing on colorectal cancer cells with overexpressing COL12A1, and the results showed that the MAPK (Mitogen-Activated Protein Kinase) pathway was significantly enriched in the COL12A1 overexpression group (Fig. 6d–f). Previous studies have shown that in gastric cancer, COL12A1 can influence the expression of IDO1 through the MAPK pathway, thereby affecting tryptophan catabolism⁴². To verify whether COL12A1 regulates IDO1 expression by affecting the MAPK pathway, we analyzed MAPK pathway protein expression in colorectal cancer cells with varying levels of COL12A1. The results showed that COL12A1 significantly affects the expression of p-ERK1/2 in the MAPK pathway (Fig. 6g). When inactive, ERK1/2 is predominantly localized in the cytoplasm; upon activation, it undergoes phosphorylation and translocates to the nucleus, subsequently modulating the activity of multiple transcription factors to regulate cellular metabolism and function⁴³. Immunofluorescence staining showed that the fluorescence intensity of p-ERK in HCT116 cells was significantly enhanced while COL12A1 overexpression, and the signals were mostly concentrated in the nucleus (Fig. 6h). Subsequently, we found that the MAPK inhibitor U0126 could significantly reverse IDO1 expression in COL12A1-overexpressing colorectal cancer cells (Fig. 6l, j). We further developed a subcutaneous tumor mice model with COL12A1-overexpressing MC38 cells, treated mice with caffeine or U0126. Results showed that inhibiting MAPK pathway restored the tumor-promoting effect of COL12A1, with consistent changes in CD8⁺ T cell infiltration and effector markers (Fig. 6k, l, Supplementary Fig. 6h). Further ELISA testing revealed that U0126 significantly reduced the Kyn levels in colorectal cancer cells and reversed the promotion of Kyn production induced by COL12A1 overexpression (Fig. 6m). The results indicated that blocking the MAPK pathway can affect the function of COL12A1 in kynurenine production. Additionally, we performed an in vitro co-culture experiment, the results demonstrated that the MAPK inhibitor significantly activated CD8⁺ T cells and counteracted the exhaustion induced by COL12A1 overexpression (Fig. 6n, Supplementary Fig. 6i). These findings suggest that COL12A1 inhibits CD8⁺ T cell activation by modulating IDO1 expression via the MAPK pathway especially activating p-ERK1/2 to impact Kyn production. However, our study on the mechanism by which COL12A1 regulates kynurenine production is only



preliminary. The specific mechanisms between ERK1/2 and IDO1, and how kynurenine regulates CD8⁺ T lymphocytes still require further investigation through subsequent experiments.

Caffeine enhances the effects of PD-1 antibody immunotherapy
Given caffeine's immune activation effect on CD8⁺ T cells, we explored its potential as an immune sensitizer by establishing a subcutaneous

tumor model with CT26 cells in BALB/c mice, treating with combination of caffeine and PD-1 antibody. Results indicated that caffeine, combined with PD-1 antibody, significantly inhibited tumor growth, improved survival times, and enhanced CD8⁺ T cell cytotoxicity and proliferation in mice (Fig. 7a–d, Supplementary Fig. 7a–d). Consistent results were obtained in a similar model using MC38 cells in C57BL/6 mice, treated with caffeine and PD-1 antibody (Fig. 7e–h,

Fig. 3 | COL12A1 is a crucial molecule in the anti-tumor effects of caffeine. Co-culture experiments of Jurkat cells treated with caffeine (0, 0.1, 1 mM). **a** Flow cytometry analysis the IFN- γ and PD-1 expression and **b** qPCR analysis of the mRNA expression of GZMB, IFNG, and PD-1, LAG3 in Jurkat cells (Representative data from $n = 3$ independent experiments). Co-culture experiments of Jurkat and HCT116 cells treated with caffeine (0, 0.1, 1 mM). **c** Flow cytometry analysis of the IFN- γ and PD-1 expression and **d** qPCR analysis of the mRNA expression of GZMB, IFNG, and PD-1, LAG3 in Jurkat cells (Representative data from $n = 3$ independent experiments). **e** Volcano plot and **f** Enrichment analysis of differentially expressed genes between caffeine-treated and control groups in HCT116 cells. **g** Venn diagram identifying COL12A1 as a gene differentially expressed in both RNA-Seq, TCGA datasets and correlated with survival outcomes. **h** qPCR analysis of COL12A1 mRNA expression and **i** western blot analysis of COL12A1 expression in paired normal and tumor tissues ($n = 12$). The samples derive from the same experiment, but different gels for COL12A1, GAPDH were processed in parallel. The quantification provided under the blots is for the representative blot from $n = 3$ independent experiments.

j Immunohistochemistry staining of COL12A1 and CD8 in colorectal cancer tissue microarray (TMA) samples, scale bars, 100 μ m, 50 μ m. Quantification of COL12A1 expression in tumors ($n = 202$, Min = 1, Max = 12, Median = 6, Lower Whisker = 1, Upper Whisker = 12, Q1 = 4, Q3 = 9, IQR = 5) compared to normal tissues ($n = 65$, Min = 0, Max = 12, Median = 4, Lower Whisker = 0, Upper Whisker = 12, Q1 = 2, Q3 = 6, IQR = 4). **k** OS plot and **l** Cox regression analysis the prognostic significance of COL12A1 expression and other clinical variables based on TMA dataset ($n = 202$). **m** Representative images of immunofluorescence co-staining for COL12A1 (red) and CD8 (green) with TMA samples; statistical plot of the number of CD8⁺ T cells (COL12A1-high, $n = 60$, Min = 12, Max = 257, Median = 78.5, Lower Whisker = 12, Upper Whisker = 257, Q1 = 46, Q3 = 143.25, IQR = 97.25; COL12A1-low, $n = 60$, Min = 45, Max = 402, Median = 168.5, Lower Whisker = 45, Upper Whisker = 402, Q1 = 129, Q3 = 235, IQR = 106). Scale bars, 100 μ m. Data error bars are mean \pm SD. The statistical analysis of **h** is Student's two-tailed paired t-test, **k** is Log-rank test, the others are Student's two-tailed unpaired t-test. The images of co-culture elements were drawn by Figdraw. Source data is provided as a Source Data file.

Supplementary Fig. 7e–h). Subsequently, we developed an orthotopic implantation model treated with a PD-1 antibody and caffeine combination. Results showed that this combination significantly inhibited tumor growth, enhanced survival, and increased CD8⁺ T cell cytotoxicity and proliferation (Supplementary Fig. 7i–n). These results indicate that caffeine has an immune-sensitizing effect and can enhance the efficacy of PD-1 monoclonal antibody immunotherapy.

Public database analysis revealed that high COL12A1 expression correlates with poor immunotherapy response and lower survival rates in various cancers (Fig. 7l, j). We further investigated the correlation between COL12A1 protein levels and immunotherapy response in CRC patients. We obtained 21 CRC samples prior to immunotherapy for IHC analysis. Results indicated that high COL12A1 expression was linked to non-responsiveness to immunotherapy, whereas responders generally had lower COL12A1 levels and higher infiltration of CD8⁺ T cells (Fig. 7k, l, Supplementary Fig. 8a). In conclusion, high COL12A1 expression may mark non-responsiveness to immunotherapy in cancer patients.

Discussion

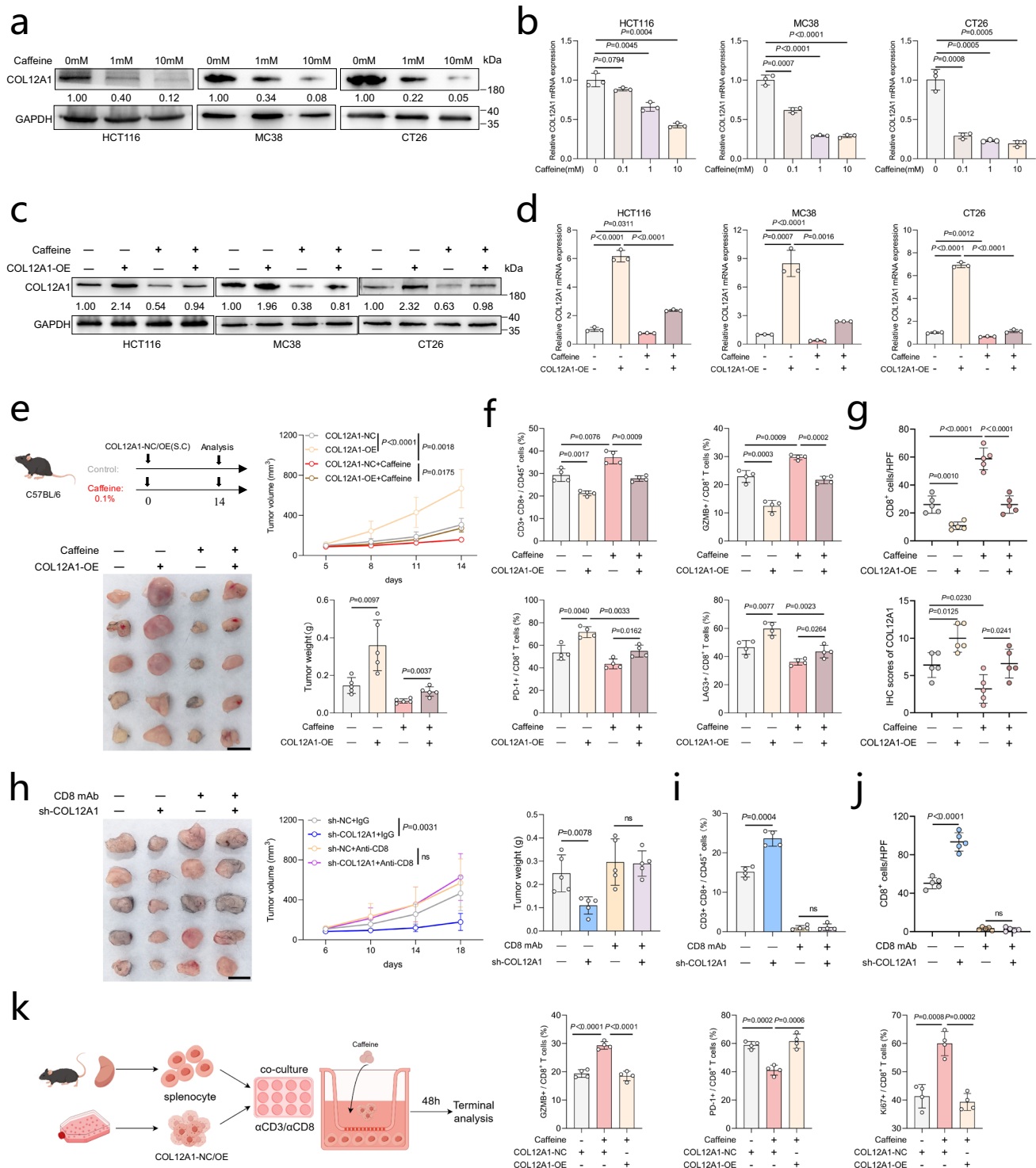
CRC remains a formidable health challenge globally, ranking as the third most common cancer and the second leading cause of cancer-related deaths. Despite its success in treating various cancers, immunotherapy shows limited efficacy in CRC, primarily benefiting patients with MSI-H. The limited responsiveness of CRC to immune checkpoint inhibitors (ICIs) underscores the need for combination therapies to broaden the population that can benefit from these treatments. Certain dietary components may enhance the effectiveness of immunotherapies. For instance, diets rich in nutrients such as serine, glycine, and methionine have been shown to alter the tumor microenvironment and immune responses^{44–46}. Similarly, other studies have shown diverse mechanisms by which dietary components modulate tumor microenvironments, our study's findings align with emerging research indicating that metabolic pathways play a significant role in tumor immunology^{47–49}. Integrating dietary strategies with immunotherapy could offer a multi-faceted approach to cancer treatment, leveraging the synergistic effects of nutrition and pharmaceutical interventions.

Our study found that beyond its traditional benefits such as reducing inflammation and regulating the gut microbiome^{15,16}, caffeine as a dietary component could enhance the immune-sensitizing effects of PD-1 inhibitors in CRC. Our findings indicate that caffeine, administered at moderate concentrations, does not significantly affect body weight, liver and spleen sizes, or serum levels of key enzymes and metabolites in treated mice. This underscores its potential as a safe component in cancer treatment regimens, particularly in combination with established immunotherapeutic drugs. Given the widespread consumption of coffee globally, caffeine presents a convenient and cost-effective strategy to complement existing therapies and broaden

treatment options for CRC patients. Although our preclinical findings demonstrate the potential of caffeine in enhancing immune responses and improving the efficacy of immunotherapy in colorectal cancer, the specific therapeutic dosage for humans remains unclear. Clinical studies suggest that moderate caffeine intake (200–400 mg per day) is generally safe and may have beneficial effects on immune function. However, the optimal dosage for cancer therapy will depend on individual factors such as metabolic rate and genetic variations in caffeine metabolism. Future clinical trials are needed to determine the precise dosage, safety, and efficacy of caffeine in combination with immunotherapy for colorectal cancer patients.

The findings in this paper significantly advance our understanding by linking caffeine's antitumor effects to specific molecular pathways, notably the downregulation of COL12A1 and the modulation of tryptophan metabolism. COL12A1, as a component of the extracellular matrix, has been implicated in various cancers and is correlated with the aggressiveness and metastatic potential of tumor^{19,21,22}. Our results found that COL12A1 is overexpressed in CRC tissues and is associated with poor prognosis. By modulating COL12A1 expression, caffeine can effectively reshape the immune landscape, enhancing the susceptibility of CRC to immunotherapies. Moreover, identifying COL12A1 as a marker of non-responsiveness to immunotherapy represents a significant advancement in understanding how tumor-expressed molecules influence treatment efficacy, as prior literature had not fully elucidated its role in immune modulation in CRC. Additionally, in most cancers COL12A1 is primarily expressed by cancer-associated fibroblasts (CAF). Consequently, knockdown of COL12A1 in cancer cells will most likely result in a modest decrease in overall COL12 levels in the TME. The interplay between tumor cells and CAF-derived COL12A1 in regulating the immune microenvironment and its impact on immunotherapy responses could be explored.

While our findings are promising, they have certain limitations. Although caffeine modulated the tumor microenvironment in animal models, translating these findings to clinical practice requires further validation. Future studies should prioritize clinical trials to evaluate the safety, optimal dosage, and efficacy of caffeine in combination with PD-1 inhibitors across diverse patient populations. Additionally, the potential variability in caffeine's effects due to individual metabolic responses and tumor heterogeneity, which were not fully explored in this study. Some individuals metabolize caffeine more rapidly than others, which could lead to differences in its immune-modulating effects. As such, future clinical studies should account for these metabolic differences when determining the optimal caffeine dosage and its effectiveness in enhancing immunotherapy, ensuring personalized and safe treatment regimens for colorectal cancer patients. Additionally, the mechanism of our research is not fully investigated and our research about the mechanism is a preliminary investigation. Investigating patient-specific factors, such as genetic variations in



caffeine metabolism, could refine treatment approaches to maximize therapeutic benefit. Moreover, the precise molecular mechanisms by which caffeine downregulates COL12A1 via KLF4 require further elucidation. Our experimental series demonstrated that KLF4 directly interacts with the COL12A1 promoter, facilitating COL12A1 transcription and functioning as an upstream regulator of COL12A1. However, the mechanism by which caffeine regulates KLF4 and subsequently affects COL12A1 remains unclear, potentially involving stress responses or transporter activation. Furthermore, our research findings indicate that caffeine treatment suppresses the glycolytic response in colorectal cancer cells. Previous studies suggest a correlation between KLF4 and glycolysis, where KLF4 may influence glycolysis, and

glycolysis could, in turn, impact KLF4. This represents a potential avenue for future investigation. The study suggests a significant link between caffeine, CD8⁺ T cells, and kynurenine production, highlighting its potential role in tumor immunity, though the specific signal pathways involved remain unclear. Therefore, this may involve deeper transcriptomic, proteomic, and metabolomic analyses to identify additional regulatory molecules and pathways influenced by caffeine. Moreover, current data suggest that caffeine may modulate COL12A1 through the MAPK-IDO1 pathway especially activating ERK1/2. Existing literature reports that ERK1/2 phosphorylation can activate transcription factors such as STAT3, NF- κ B and AP-1⁴³, which could regulate IDO1 expression under specific conditions, particularly during

Fig. 4 | Caffeine activates CD8⁺ T cells by KLF4/COL12A1 axis in CRC cells.

a Western blot and **b** qPCR analysis of COL12A1 expression in CRC cells treated with caffeine (0, 1, 10 mM) (Representative data from $n = 3$ independent experiments). The samples derive from the same experiment but different gels for COL12A1, GAPDH were processed in parallel. The quantification provided under the blots is for the representative blot from $n = 3$ independent experiments. **c** Western blot and **d** qPCR analysis COL12A1 expression in COL12A1-overexpressed (COL12A1-OE) and control cells treated with caffeine (1 mM) (Representative data from $n = 3$ independent experiments). The samples derive from the same experiment but different gels for COL12A1, GAPDH were processed in parallel. The quantification provided under the blots is for the representative blot from $n = 3$ independent experiments. **e** Schematic depicting the treatment of caffeine in subcutaneous COL12A1-OE MC38 tumor-bearing C57BL/6 mice. Representative images of tumor from caffeine-treated or COL12A1-OE groups ($n = 5$ per group). Scale bars, 1 cm. Quantification of the tumor growth curve and tumor weight. **f** Flow cytometry analysis of CD8⁺ T cells and GZMB, PD-1, LAG3 expression ($n = 4$ per group) or **g** Quantification of

immunohistochemistry staining of CD8⁺ T cells and COL12A1 ($n = 5$) in tumor of subcutaneous MC38 with COL12A1-OE or control (COL12A1-NC) tumor-bearing C57BL/6 mice treated with caffeine or control. **h** Representative images of tumors from the treatment of anti-CD8 monoclonal antibody (CD8 mAb) (200 μ g, ip, twice weekly) in subcutaneous MC38 with COL12A1 knockdown (sh-COL12A1) or control (sh-NC) tumor-bearing C57BL/6 mice ($n = 5$ per group). Scale bars, 1 cm. Quantification of the tumor growth curve and tumor weight. **i** Flow cytometry analysis ($n = 4$ per group) and **j** Quantification of immunohistochemistry staining ($n = 5$) of CD8⁺ T-cell infiltration in subcutaneous MC38 with sh-COL12A1 tumor-bearing C57BL/6 mice treated with CD8 mAb. **k** Schematic of co-culture experiments with splenocytes and COL12A1-OE MC38 cells treated with caffeine (1 mM). Flow cytometry analysis the GZMB, PD-1 and Ki67 expression in CD8⁺ T cells of splenocytes ($n = 4$ per group). Data error bars are mean \pm SD. The statistical analysis of the growth curve is Two-way ANOVA, the others are Student's two-tailed unpaired t-test. The images of mice and co-culture elements were drawn by Figdraw. Source data is provided as a Source Data file.

inflammation and immune responses^{50–52}. Therefore, we hypothesize that COL12A1 promotes the phosphorylation and nuclear translocation of ERK1/2, subsequently activating transcription factors to regulate IDO1 expression, but the precise signaling events between ERK1/2 and IDO1 need to be explored in more detail. Future studies should focus on pinpointing the specific molecular targets and mechanisms involved in this process to better understand how caffeine influences tumor immunity and its potential as a therapeutic adjunct in cancer treatment. Understanding these interactions could uncover potential drug targets and combination strategies. The study used a controlled caffeine dosage in mice, but determining the optimal dosage and administration method in humans could be challenging, as caffeine's effects may vary based on individual metabolism and consumption habits.

In conclusion, this study makes a significant contribution to cancer immunotherapy by suggesting that dietary components, such as caffeine, a widely consumed substance, may enhance the effectiveness of PD-1 blockade in CRC. Our study underscores caffeine's potential as a dietary intervention that can significantly enhance immunotherapy efficacy in CRC by modulating the COL12A1/IDO1/Kyn axis. Caffeine's capacity to modulate the immune microenvironment and sensitize tumors to immunotherapy raises the possibility that other dietary components could similarly enhance cancer treatment outcomes. This study develops combination therapies that leverage dietary components to improve cancer outcomes, presenting a non-invasive and easily integrated strategy to enhance immunotherapy outcomes. Further research in this area could lead to more personalized and effective treatment strategies for CRC patients, potentially transforming the current landscape of cancer therapy.

Methods

Ethics statement

This study was approved by the Medical Ethics Committee of NanFang Hospital of Southern Medical University (NFEC-2021-396). The experiments were undertaken with the understanding and written consent of each participant, which was in accordance with the Declaration of Helsinki. The use of excised human specimens was approved by the Institute Research Medical Ethics Committee of Nanfang Hospital (Guangzhou, China). All mouse care, protocol and experiments were approved by the Animal Research Ethics Committee of Southern Medical University (SMUL2022189), and all animals received humane care according to the standards outlined in the Guide for the Care and Use of Laboratory Animals.

Mice

Female athymic nude femice (BALB/c-nu/nu, 6 weeks old), female C57BL/6j mice (6 weeks old), and female BALB/c mice (6 weeks old) were purchased from the animal center (Guangdong Province, China)

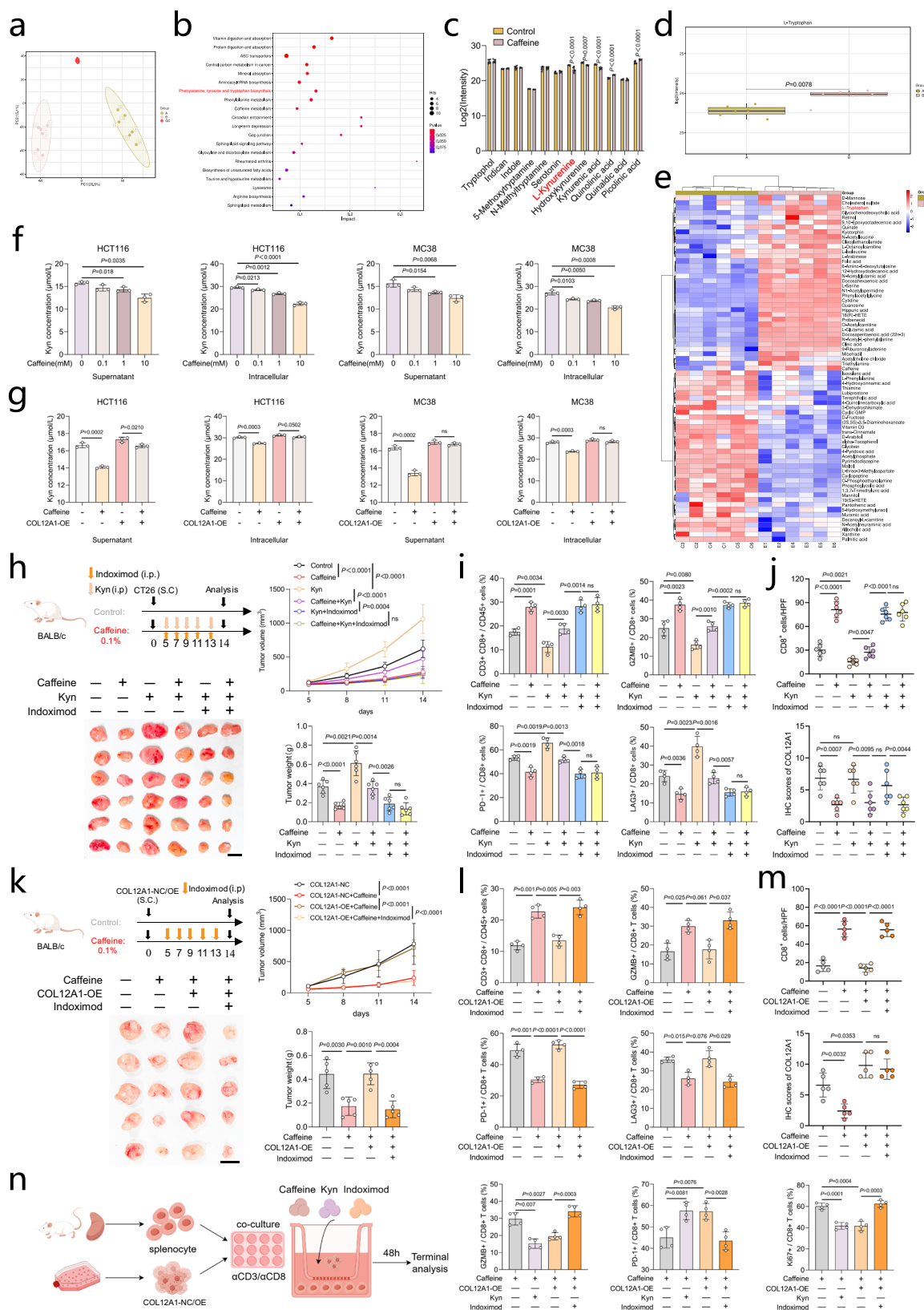
for use as subcutaneous xenograft models or orthotopic implant models. The APC^{Min/+} mice were purchased from the GENECHM Biotech at Shanghai (<http://genechem.bioon.com.cn/>) and the mouse genotypes were detected with PCR. Only female mice were used in the experiments to ensure the reproducibility of tumor kinetics and growth (without gender bias). Mice were housed in specific pathogen free (SPF) conditions, at a suitable temperature (18–23 °C) and humidity (22–50%) under a 12/12-h light/dark cycle, with 4–5 mice per cage. All animals were allowed to eat (AIN-93 standardized feed) and drink freely during the experiment.

Human specimens

12 paired fresh CRC tissues and adjacent normal mucosa were collected and stored in liquid nitrogen to analyze the mRNA levels of COL12A1 via qPCR, the protein expression of COL12A1 by western blot and the Kyn concentration by ELISA. The tissue microarray (TMA), involving a total of 202 CRC patients who underwent colorectal resection from November 2013 to June 2014 in Nanfang Hospital, Southern Medical University (Guangzhou, China). We collected the patient information about gender, age, BMI, pathology stage, tumor differentiation, and overall survival of the TMA (detail information presented in Source Data F3j). 21 CRC specimens prior to anti-PD-1 immunotherapy were used for IHC analysis, which were collected from the Department of Radiation Oncology, NanFang Hospital, Southern Medical University. We additionally collected information about treatment regimens, duration and response of therapy for all immunotherapy-treated patients (detail information presented in Source Data F7k). Tumor response was assessed according to the Modified Response Evaluation Criteria in Solid Tumor. Sex and gender of participants was determined based on self-report and clinical report.

Tumor growth and treatment

For the subcutaneous tumor xenograft models, CT26 colon cancer cells (5×10^5 cells or 1×10^6 per animal) or MC38 colon cancer cells (5×10^5 cells or 1×10^6 per animal) were subcutaneously (s.c.) injected into experimental mice to form solid tumors. Tumor diameters were measured every three or four days, and tumor volume (mm^3) = (length \times width²)/2 was used to evaluate the tumor volumes. For the orthotopic xenograft CRC mouse model, CT26 (5×10^5 cells per animal) were orthotopically injected (o.i.) into the wall of the cecum in BALB/c mice. After 14 days, all the mice were sacrificed. Colons were harvested to assess the tumor burden. The tumor load was less than the maximum diameter (20 mm for subcutaneous tumor xenograft models, 30 mm for orthotopic tumor xenograft models) approved by the University Animal Research Ethics Committee of Southern Medical University. All tumors in the experiment did not exceed the limit. Tumors were excised and rapidly placed in formalin or liquid nitrogen



for IHC or qRT-PCR. The venous blood of mice was drawn from the eye orbit to evaluate ALT, AST, BUN and CREA levels.

The treatments were designed as follows: (1) Caffeine (Cat. No. C0750, Sigma-Aldrich) was given in 0.1% w/v drinking water (2) InVivo MAb anti-CD8α antibody (Cat. No. A2108, Selck) was given 200 μg/mouse intraperitoneally twice weekly; (3) Kyn (Cat. No. K8625, Sigma-

Aldrich) was given 100 mg/kg intraperitoneally every two days; (4) Indoximod (Cat. No. S7756, Selck) was given 100 mg/kg intraperitoneally every two days; (5) U0126 (Cat. No. S1102, Selck) was given 15 mg/kg intraperitoneally every three days; (6) InVivo MAb anti-mouse PD-1 (Cat. No. A2122, Selck) was given 10 mg/kg intraperitoneally twice weekly.

Fig. 5 | Caffeine downregulates COL12A1 to reduce kynurenine. **a** Principal component analysis, **b** Enrichment analysis of metabolites, **c** Quantification of tryptophan related metabolite levels ($n = 6$), **d** Box plots of tryptophan changes from supernatant of control (A, $n = 6$, Min=23.3397, Max = 23.7274, Median = 23.5581, Lower Whisker = 23.3997, Upper Whisker= 23.7274, Q1 = 23.4511, Q3 = 23.6636, IQR = 0.2125) and caffeine-treated (B, $n = 6$, Min = 23.5735, Max = 24.0682, Median = 23.9736, Lower Whisker=23.5735, Upper Whisker=24.0682, Q1 = 23.9351, Q3 = 24.0298, IQR = 0.1026) HCT116 cells, **e** Heatmap of differential metabolite, **f** ELISA analysis kynurenine (Kyn) levels in CRC cells treated with caffeine (0, 0.1, 1, 10 mM) (Representative data from $n = 3$ independent experiments), **g** ELISA analysis Kyn levels in COL12A1-overexpressed (COL12A1-OE) CRC cells treated with caffeine (1 mM) (Representative data from $n = 3$ independent experiments), **h** Schematic depicting the treatment of caffeine or Kyn (100 mg/kg, ip) or Indoximod (100 mg/kg, ip) in subcutaneous CT26 tumor-bearing BALB/c mice. Representative images of tumors ($n = 6$ per group). Scale bars, 1 cm. Quantification of the tumor growth curve and weight. **i** Flow cytometry analysis of CD8⁺ T cells and GZMB, PD-1, LAG3 expression ($n = 4$ per group) or **j** Quantification of

immunohistochemistry staining of CD8⁺ T cells and COL12A1 ($n = 6$) in tumor of subcutaneous CT26 tumor-bearing BALB/c mice treated with caffeine or Kyn or Indoximod or control. **k** Schematic depicting the treatment of caffeine or Indoximod in subcutaneous COL12A1-OE CT26 tumor-bearing BALB/c mice. Representative images of tumors ($n = 5$ per group). Scale bars, 1 cm. Quantification of the tumor growth curve and weight. **l** Flow cytometry analysis of CD8⁺ T cells and GZMB, PD-1, LAG3 expression ($n = 4$ per group) or **m** Quantification of immunohistochemistry staining of CD8⁺ T cells and COL12A1 ($n = 5$) in tumor of subcutaneous COL12A1-OE CT26 tumor-bearing BALB/c mice treated with caffeine or Indoximod. **n** Schematic of co-culture experiments with splenocytes and COL12A1-OE CT26 cells treated with caffeine (1 mM), Kyn (100 μ M) or Indoximod (50 μ M). Flow cytometry analysis of the GZMB, PD-1, Ki67 expression in CD8⁺ T cells of splenocytes ($n = 4$ technical replicates, Representative data from $n = 3$ independent experiments). Data error bars are mean \pm SD. The statistical analysis of the tumor growth curve is Two-way ANOVA, the others are Student's two-tailed unpaired t-test. The images of mice and co-culture elements were drawn by Figdraw. Source data is provided as a Source Data file.

UK Biobank

This study selected 9232 colorectal cancer patients from the UK Biobank database (Project-92668), using daily coffee consumption (in cups) as the independent variable, and analyzed factors such as BMI, gender, income, Townsend deprivation index, smoking, and alcohol consumption as covariates. After excluding samples with missing data, a final total of 7022 patients were included. Based on daily coffee consumption, patients were divided into two groups: the high caffeine intake group (more than 6 cups per day, 5022 patients) and the low caffeine intake group (6 cups or fewer per day, 1990 patients). After propensity score matching based on the above covariates, the sample size for each group was adjusted to 1981. Finally, Kaplan-Meier curves were used to perform a prognostic analysis of the two groups.

Cell culture and construction of stable cell lines

Human T cell leukemia cell line (Jurkat, ATCC TIB-152), human CRC cell line (HCT116, ATCC CCL-247) and mouse CRC cell line (CT26, ATCC CRL-2638) were purchased from the American Type Culture Collection (ATCC), mouse CRC cell line (MC38, TCM-46) was purchased from the Cell Bank of the Chinese Academy of Sciences (Shanghai). All cells were cultured in RPMI1640 medium (Gibco) or Dulbecco's Modified Eagle Medium (DMEM) (Gibco), supplemented with 10% fetal bovine serum (Gibco), 100U/ml penicillin and 100 μ g/ml streptomycin (Gibco). All cell were cultured at 37 °C in an atmosphere containing 5% CO₂. All cell lines used in this study had been authenticated by STR profiling and tested for mycoplasma contamination.

Adenoviral vectors were designed and constructed by WZ Biotech (Beijing, China). Lentiviral vectors were designed and constructed by YIJIN Biotech (Guangzhou, China). Flag-tagged COL12A1-overexpression vectors (Ad-COL12A1) and control vectors (Ad-NC) were transfected into HCT116, MC38 and CT26 cells. COL12A1 short hairpin RNA (sh-COL12A1) and control short hairpin RNA (sh-NC) were transfected into HCT116, MC38 and CT26 cells to generate COL12A1-knockdown cells. Transfection was performed according to the manufacturer's protocols.

Isolation of tumor-infiltrating cells and splenocytes

For single-cell suspension preparation, spleens and tumors of mice were harvested in DMEM medium containing 1% bovine serum albumin. Tumor tissues were cut and collected in DMEM medium supplemented with 0.5 mg/ml collagenase IV (Sigma-Aldrich) and 0.1 mg/ml deoxyribonuclease type I (Sigma-Aldrich), incubated for 1 h at 37 °C in a shaker, and then mechanically dissociated on frosted glass slides. Harvested spleens were directly mechanically separated on frosted glass slides. Tumor or splenocyte suspensions were filtered through a 70 μ m cell filter (Solarbio Life Science, China) to obtain single-cell suspensions. Erythrocytes were lysed with ACK

buffer (Solarbio) for 2 min at room temperature, then terminate the lysis with DMEM.

Flow cytometry

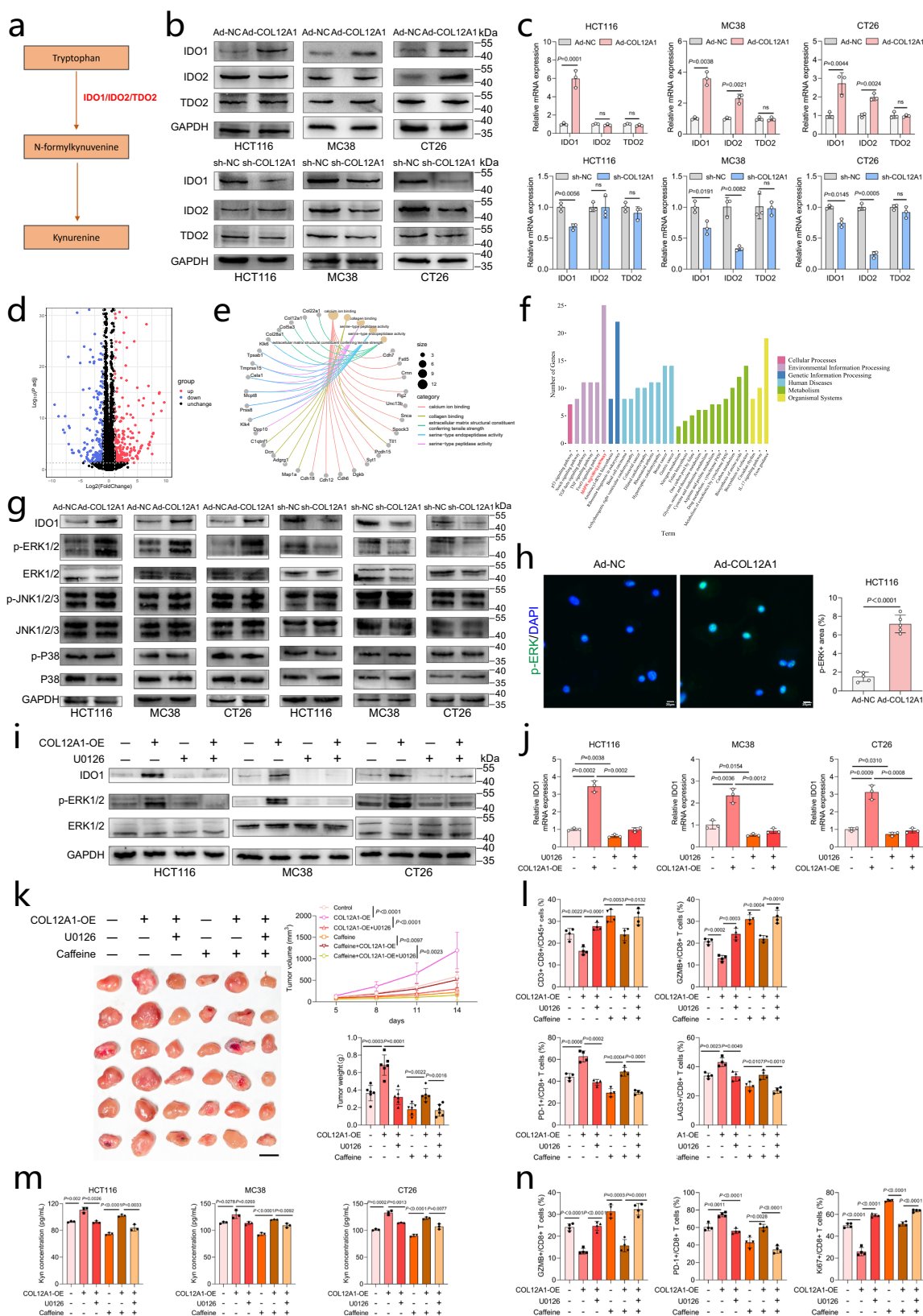
For flow cytometry analyses, surface staining or intracellular staining were processed and analyzed using BD LSRFortessa X-20 Cell Analyzer (BD Biosciences, USA). Cells collected from culture dishes or transplanted tumors were centrifuged at 300 \times g for 5 min and washed in HBSS. The cells were transferred to 1.5 mL EP tubes and centrifuged at 300 \times g for 8 minutes. Then, 200 μ L buffer II was added to the tube with antibodies (the specific antibodies used are listed in Supplementary Table 1). The cells were incubated for 30 min at 4 °C in the dark. Then the cells were then centrifuged at 300 \times g for 8 min and washed in buffer II. For intracellular protein, permeabilization buffer (Cat No. 554714, BD Biosciences, USA) was used before staining with antibodies (the specific antibodies used are listed in Supplementary Table 1). Samples were fixed in 1% paraformaldehyde and stored at 4 °C in the dark. A BD Biosciences LSRFortessa (Special Order Research Product) was acquired to detect the samples. The flow cytometry data analysis was performed with FlowJo v10.4.

Western blot

Cells or tissues were lysed with RIPA buffer (Amresco, USA) containing a protease and phosphatase inhibitors (Leagene, China). Total proteins were separated using 10% sodium dodecyl sulfate-polyacrylamide gel electrophoresis (VWR Life Science, USA) and transferred to polyvinylidene fluoride membranes (Millipore, USA). The membranes were then probed with primary antibodies (the specific antibodies used are listed in Supplementary Table 1), followed by incubation with secondary antibodies (the specific antibodies used are listed in Supplementary Table 1) conjugated with HRP. The signal was detected using enhanced chemiluminescence (FD Bio-pico ECL, China). All results are derived from at least three independent biological replicates, and representative results are shown. Protein levels were quantified by densitometry using ImageJ software. Tubulin or GAPDH served as the internal control as indicated in the figures. The antibodies used in the research are specificity for both human and murine proteins. The original data of western blot was supplied in the Source Data file.

Quantitative real-time PCR

Total RNA from cells was extracted using TRIzol reagent (TaKaRa, Japan), according to the manufacturer's instructions. The total RNA was then reverse-transcribed into cDNA using a PrimeScript RT-PCR Kit (TaKaRa, Japan). The expression of mRNA was analyzed using SYBR Premix Ex Taq (TaKaRa) with a LightCycler 96 Detection System (Roche) using GAPDH for normalization. qPCR was performed using the primers listed in Supplementary Table 2.



Immunohistochemistry

IHC staining was performed according to previously described standard protocols¹⁰. Sections were deparaffinized with xylene, rehydrated, subjected to heat-mediated antigen retrieval, and blocked with 3% hydrogen peroxide, followed by incubating in primary antibodies (the specific antibodies used are listed in

Supplementary Table 1) overnight at 4 °C. Next day, the sections were put in room temperature for 30 min to rewarm, followed by secondary antibody incubation for 1 h at room temperature. The visualization signal was stained with 3, 3'-diaminobenzidine (DAB) and then counterstained with hematoxylin. The images were taken with OLYMPUS DP22 microscope (Olympus, Japan) and to assessed

Fig. 6 | COL12A1 regulates Kyn production via MAPK-IDO1 axis. **a** Schematic of tryptophan-kynurenine pathway. **b** Western blot and **c** qPCR analysis of the expression of IDO1, IDO2, and TDO2 in CRC cells with COL12A1 overexpression (Ad-COL12A1) and knockdown (sh-COL12A1) (Representative data from $n = 3$ independent experiments). The samples derive from the same experiment but different gels for IDO1, IDO2, another for TDO2 and another for GAPDH were processed in parallel. **d** Volcano plot, **e** Enrichment analysis and **f** KEGG analysis in Ad-COL12A1 MC38 cells compared to control. **g** Western blot analysis of ERK1/2, JNK1/2/3, p38, and IDO1 in CRC cells with different COL12A1 expression. The samples derive from the same experiment, but different gels for IDO1, p-ERK1/2, another for ERK1/2, another for p-JNK1/2/3, another for JNK1/2/3, another for p-P38, another for P38 and another for GAPDH were processed in parallel. **h** Representative fluorescence images and quantitative analysis of p-ERK (green) in Ad-COL12A1 HCT116 cells (Representative images from $n = 5$ independent experiments). Scale bars, 20 μm . **i** Western blot analysis the expression of IDO1 and ERK1/2 levels and **j** qPCR analysis the expression of IDO1 in COL12A1-OE CRC cells treated with U0126 (5 μM)

(Representative data from $n = 3$ independent experiments). The samples derive from the same experiment but different gels for IDO1, p-ERK1/2, another for ERK1/2 and another for GAPDH were processed in parallel. **k** Schematic depicting the treatment of caffeine or U0126 in subcutaneous COL12A1-OE MC38 tumor-bearing C57BL/6 mice ($n = 6$ per group). Scale bars, 1 cm. Quantification of the tumor growth curve and tumor weight. **l** Flow cytometry analysis of CD8⁺ T cells and GZMB, PD-1, LAG3 expression ($n = 4$) in tumor of Fig. 6k. **m** ELISA analysis of kynurenine (Kyn) levels in COL12A1-OE CRC cells treated with caffeine (1 mM) or U0126 (5 μM) (Representative data from $n = 3$ independent experiments). **n** Flow cytometry analysis the GZMB, PD-1, Ki67 expression in CD8⁺ T cells of splenocytes co-cultured with COL12A1-OE MC38 cells treated with caffeine (1 mM) or U0126 (5 μM) ($n = 4$ technical replicates, Representative data from $n = 3$ independent experiments). Data error bars are mean \pm SD. The statistical analysis of the tumor growth curve is Two-way ANOVA, the others are Student's two-tailed unpaired t-test. Source data is provided as a Source Data file.

the expression of indicated markers by two pathologists separately. At least three individual fields (20 \times magnification) were chosen to estimate the score of each slide. Next, a final score was calculated by multiplying the proportion of positively stained tumor cells (0–100%) by the staining intensity (0, 1, 2, or 3). As for the detection index of immune cell marker like CD8A, the numbers of CD8-positive cells should be counted under a high-power microscope.

ELISA

ELISA were performed according to the manufacturer's instructions of ELISA kits. The mean O.D. values for each standard and sample were calculated. A standard curve was constructed to determine the concentration of the samples.

Serum AST, ALT, BUN and CREA measurement

Serum levels of AST, ALT, BUN, and CREA were quantified using an Automatic Clinical Chemistry Analyzer (Chemray 800, Shenzhen Rayto Life Technology Co., Ltd) to assess the toxicological impact of caffeine on hepatic injury and renal dysfunction in mice. AST was measured with the alanine aminotransferase kit (S03030, Rayto), ALT with the aspartate aminotransferase kit (S03040, Rayto), BUN with the blood urea nitrogen test kit (S03046, Rayto), and CREA with the creatinine assay kit (S03076, Rayto).

CD8⁺ T-cell isolation and activation

C57BL/6 mice, aged 6–8 weeks, were euthanized under anesthesia. Following immersion in 75% ethanol, the spleen was excised and fragmented into small segments. These fragments were mechanically dissociated using 70 μm strainers (Cat No. 15-070, BIOLOGIX, USA), flushed with PBS supplemented with 2% FBS, and collected. After centrifugation at 350 \times g for 10 min, the cell pellet was resuspended in PBS and adjusted to a concentration of 1×10^8 cells/ml. CD8⁺ T cells were isolated using an EasySep Mouse CD8⁺ T-Cell Isolation Kit (Cat No. 11417D, ThermoFisher, USA) according to the manufacturer's instructions. The purified T cells were then seeded into a 6-well plate precoated with 1 $\mu\text{g}/\text{mL}$ anti-CD3 antibody (Cat No. 05112-25-500, BioGems, USA) and cultured for 3–5 days.

Chromatin Immunoprecipitation (ChIP) assay

ChIP assays were conducted using a ChIP Kit (Abcam, ab500) in accordance with the manufacturer's protocol. Briefly, cells were cultured and fixed with 1% formaldehyde at room temperature for 10 min to cross-link histone and non-histone proteins to DNA, followed by quenching with glycine. Chromatin was enzymatically digested and sonicated to generate DNA/protein fragments ranging from 150 to 900 bp. Immunoprecipitation was performed using an antibody specific to KLF4 (Cat. 11880-1-AP, Proteintech), with the resulting complexes captured by Protein A/G beads. Cross-links were subsequently

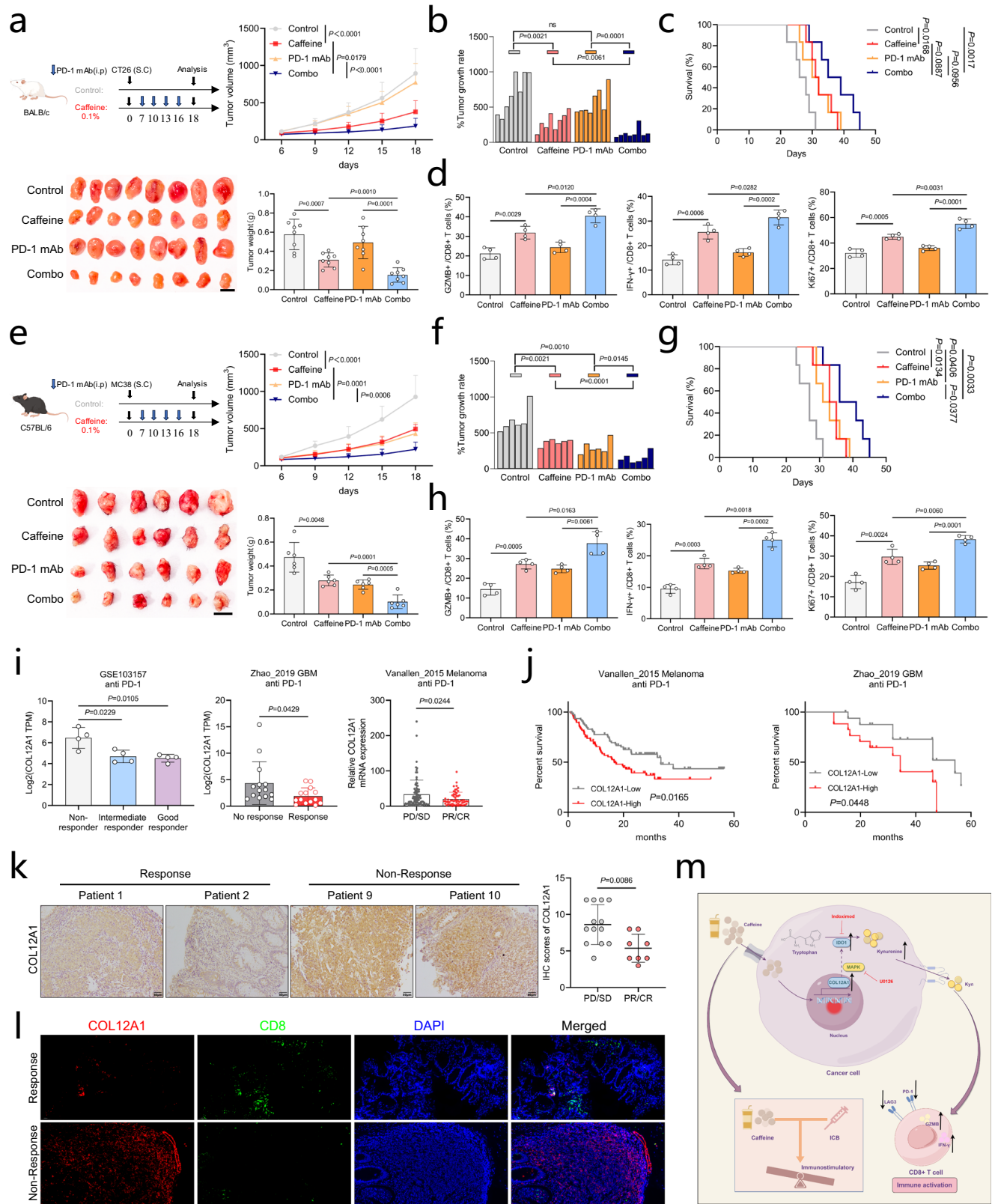
reversed, and target DNA fragments were purified using a DNA purification slurry. The interaction between the COL12A1 promoter and KLF4 or IgG was quantified via quantitative PCR, with PCR products analyzed by agarose gel electrophoresis. Primer sequences used for ChIP are detailed in Supplementary Table 2.

Dual-Luciferase reporter assay

HEK-293T cells were suspended and plated at a density of 1×10^4 cells per well in 96-well plates. Putative KLF4 binding sites within the COL12A1 promoter were identified using the JASPAR database (<https://jaspar.elixir.no/>). Upon reaching 60%–70% confluence, a Dual-Luciferase Reporter Assay was conducted to investigate the interaction between KLF4 and the COL12A1 promoter. Fragments of the COL12A1 promoter region (Full, Mut1, Mut2, and Mut3) were cloned into the pGL4-Basic vector, while KLF4 was inserted into the pcDNA3.1 vector (GenePharma, China). Firefly luciferase plasmids containing h-COL12A1 (WT, Mut1, Mut2, and Mut3) or pGL4-Basic (negative control) were co-transfected with KLF4 expression vectors (pcDNA3.1) and the pRL-TK Renilla luciferase vector (internal control) into HEK-293T cells. After 48 hours, cell lysates were harvested, and firefly and Renilla luciferase activities were measured using Dual-Luciferase Reporter Assay Kits (GenePharma, China). Luminescence signals were quantified with a multifunctional microplate reader (SuPerMax3100, Shanghai Flash Spectrum Biological Technology Co., Ltd, China). The experiment was performed in triplicate.

Multi-color immunofluorescence

The multi-color immunofluorescence was performed with a three-color multiplex fluorescent immunohistochemical staining kit (Cat. No. AFIHC033, AiFang, China) according to the manufacturer's protocol. In brief, sections were subjected to microwave-induced antigen retrieval in Tris-EDTA buffer (pH=9.0) and submerged into 3% hydrogen peroxide for blocking endogenous peroxidase activity. Sections were washed in TBST and blocked with goat serum for 30 min, followed by incubating with primary antibody (listed in Supplementary Table 1) for 1 h at room temperature, and slides were washed in TBST. Horseradish peroxidase-labeled goat anti-rabbit/mouse secondary antibody was used and developed with fluorescent dye diluted by the signal amplification reagent provided by the kit. For multiple fluorescent staining, sections were processed starting from the antigen retrieval step to remove binding antibodies, and then incubated with another primary antibody. This was repeated until all antigens were stained. Finally, counterstaining was performed with DAPI and anti-fluorescence quenching blocker was added dropwise. The images were taken with Zeiss LSM 880 confocal laser scanning microscope (Zeiss, Germany) and analyzed fluorescence intensity or positive cells numbers using ZEN microscopy software.



Co-culture system

Tumor cell culture supernatant (TSN) was prepared by culturing tumor cells in DMEM or RPMI-1640 containing 1% FBS for 48 h. The TSN was then centrifuged at 450×g for 10 min and harvested. Prior to co-culture, splenocytes or mouse CD8⁺ T cells were isolated from C57BL/6 or BALB/c mice spleen and activated with plate-bound anti-mouse CD3 (5 μg/ml) and soluble anti-mouse CD28 (1 μg/ml), and then implanted

at the lower 24-well plates for two days. Next, MC38 or CT26 cells mixed with splenocytes or mouse CD8⁺ T cells in a 2:1 ratio were seeded in the upper of the 0.4 μm transwell insert (Corning, USA). Then we added caffeine, Kyn, Indoximod or U0126 in the upper of the transwell insert. After 48 hours, splenocytes or mouse CD8⁺ T cells were collected and stained with antigen antibodies for flow cytometry or qPCR analyses.

Fig. 7 | Caffeine enhances the effects of PD-1 antibody immunotherapy.

a Schematic depicting the treatment of caffeine (0.1% w/v, daily) or anti-PD-1 monoclonal antibody (PD-1 mAb, 10 mg/kg, ip, twice weekly) in subcutaneous CT26 tumor-bearing BALB/c mice. Representative images of tumor from caffeine-treated or PD-1 mAb groups ($n = 8$). Scale bars, 1 cm. Quantification of the tumor growth curve and tumor weight. **b** Waterfall plot on tumor volume changes ($n = 8$) and **c** Kaplan-Meier survival curves of subcutaneous CT26 tumor-bearing BALB/c mice treated with caffeine, PD-1 mAb, or their combination ($n = 6$). **d** Flow cytometry analysis of GZMB, IFN- γ , Ki67 of CD8 $^{+}$ T cells in tumor of subcutaneous CT26 tumor-bearing BALB/c mice treated with caffeine, PD-1 mAb, or their combination ($n = 4$). **e** Schematic depicting the treatment of caffeine or PD-1 mAb in subcutaneous MC38 tumor-bearing C57BL/6 mice. Representative images of tumor from caffeine-treated or PD-1 mAb groups ($n = 6$). Scale bars, 1 cm. Quantification of the tumor growth curve and tumor weight. **f** Waterfall plot on tumor volume changes ($n = 6$) and **g** Kaplan-Meier survival curves of subcutaneous MC38 tumor-bearing C57BL/6 mice treated with caffeine, PD-1 mAb, or their combination ($n = 6$). **h** Flow cytometry

analysis of GZMB, IFN- γ , Ki67 of CD8 $^{+}$ T cells in tumor of subcutaneous MC38 tumor-bearing C57BL/6 mice treated with caffeine, PD-1 mAb, or their combination ($n = 4$). **i** Analysis of mRNA expression of COL12A1 associated with response to anti-PD-1 therapy in multiple cancers in public datasets, Zhao_2019_GBM, (PRJNA482620, $n = 14$), Vanallen_2015_Melanoma (PHS000452, PD/SD, $n = 66$, PR/CR, $n = 39$). **j** Kaplan-Meier survival analysis of patients treated with anti-PD-1 therapy in public datasets. **k** Immunohistochemistry staining and quantification of COL12A1 in pre-immunotherapy CRC samples from responders ($n = 8$) and non-responders ($n = 13$), scale bar, 50 μ m. **l** Representative images of immunofluorescence co-staining for COL12A1 (red) and CD8 (green) in pre-immunotherapy CRC samples from responders and non-responders. Representative images from $n = 6$ independent experiments. Scale bar, 50 μ m. **m** Schematic diagram. Data error bars are mean \pm SD. The statistical analysis of growth curve is Two-way ANOVA, survival curve is Log-rank test, the others are Student's two-tailed unpaired t-test. The images of mice elements and the schematic diagram of graphical abstract were drawn by Figdraw. Source data are provided as a Source Data file.

Seahorse assay

Oxygen consumption rate (OCR) was determined using a Seahorse XFe 96 Extracellular Flux Analyzer with the Agilent Seahorse XF Cell Mito Stress Test Kit (Agilent, 103015-100). Briefly, colorectal cancer (CRC) cells were seeded into XF96-well culture plates, treated with 1 mM caffeine, and incubated at 37°C overnight prior to analysis. Mitochondrial function was evaluated by sequential addition of oligomycin, FCCP, and a combination of rotenone and antimycin A, following the manufacturer's instructions. Extracellular acidification rate (ECAR) was assessed using the XF Glycolysis Stress Test Kit (Agilent, 103020-100) protocol, with sequential administration of glucose, oligomycin, and 2-deoxyglucose (2-DG). Data were analyzed using Seahorse Wave software. Post-assay, cells in each well were trypsinized and counted for normalization of results. Non-mitochondrial OCR and non-glycolytic acidification were subtracted during quantification.

Immunofluorescence staining

According to routine protocols, prepared cell samples were treated with 3% H₂O₂ for 10 min. Following three washes with PBS, the samples were blocked with 3% bovine serum albumin (BSA) and 0.3% Triton X-100 for 1 h, then incubated with primary antibody overnight at 4°C. After additional PBS washes, the samples were incubated with the corresponding fluorescent secondary antibody for 1 h at 37°C. Nuclei were counterstained with DAPI. Images were subsequently captured using a fluorescence microscope (Olympus BX51). Details of primary antibodies and their dilutions are provided in Supplementary Table 1.

RNA sequencing

The extraction and purification of total RNA, library construction, and sequencing were conducted by Guangzhou RiboBio Corp, China. The quality of the RNA libraries was evaluated using an Agilent 2200 TapeStation (Agilent Technologies, USA). Library sequencing was performed using a HiSeq 3000 sequencing platform (Illumina, USA).

Untargeted metabolomics Assay

We treated HCT116 with or without caffeine (1 mM) for 3 days, and collected supernatants from caffeine-treated and untreated tumor cells ($n = 6$, biological replicates). The extraction and purification of total metabolite and sequencing were conducted by Suzhou PANOMIX Corp, China. The samples were quality controlled. Following the instruction manual, brief, the processes were divided into 4 steps: (1) Metabolite extraction; (2) Standard solution preparation; (3) LC-MS analysis; (4) Data analysis. The LC analysis was performed on a Vanquish UHPLC System (Thermo Fisher Scientific, USA). Chromatography was carried out with an ACQUITY UPLC[®] HSS T3 (2.1 \times 100 mm, 1.8 μ m) (Waters, Milford, MA, USA). The column maintained at 40°C. The flow rate and injection volume were set at 0.3 mL/min and 2 μ L, respectively. For LC-ESI (+)-MS analysis, the mobile phases consisted of

(B2) 0.1% formic acid in acetonitrile (v/v) and (A2) 0.1% formic acid in water (v/v). Separation was conducted under the following gradient: 0–1 min, 8% B2 ; 1–8 min, 8–98% B2 ; 8–10 min, 98% B2 ; 10–10.1 min, 98–8% B2 ; 10.1–12 min, 8% B2. For LC-ESI (-)-MS analysis, the analytes was carried out with (B3) acetonitrile and (A3) ammonium formate (5 mM). Separation was conducted under the following gradient: 0–1 min, 8% B3 ; 1–8 min, 8–98% B3 ; 8–10 min, 98% B3 ; 10–10.1 min, 98–8% B3 ; 10.1–12 min, 8% B3. Mass spectrometric detection of metabolites was performed on Orbitrap Exploris 120 (Thermo Fisher Scientific, USA) with ESI ion source. Simultaneous MS1 and MS/MS (Full MS-ddMS2 mode, data-dependent MS/MS) acquisition was used. The parameters were as follows: sheath gas pressure, 40 arb; aux gas flow, 10arb; spray voltage, 3.50 kV and -2.50 kV for ESI(+) and ESI(-), respectively; capillary temperature, 325°C; MS1 range, m/z 100–1000; MS1 resolving power, 60000 FWHM; number of data dependant scans per cycle, 4; MS/MS resolving power, 15,000 FWHM; normalized collision energy, 30%; dynamic exclusion time, automatic. Analysis was accomplished using triple quadrupole mass spectrometry in Multiple Reaction Monitoring (MRM) mode. The software Analyst 1.6.3 was utilized to process the mass spectrometry data.

Statistics & Reproducibility

All assays were performed in at least three independent experiments. All analyses were performed using SPSS software (version 26.0) or GraphPad Prism (version 8.0). Before conducting statistical analysis, normality and homogeneity of variance tests were conducted first. Results are presented as mean \pm SD. Survival curves were generated using the Kaplan-Meier method and compared using the log-rank test. Correlation analysis was assessed using the Pearson correlation coefficient. A two-tailed unpaired Student's t-test was used to compare the variables of the two groups. Paired two-tailed Student's t-test was performed to analyze the statistical significance of matched tissue samples. Chi-square tests were performed to analyze the correlation between gene expression and clinical characteristics. Two-way analysis of variance (ANOVA) was performed for multi-group comparisons. Statistically significance was set at $p < 0.05$. ns, no significant difference. The experiments were not randomized, except that mice were randomly grouped before different treatments. Data collection and analysis were not performed blind to the conditions of the experiments, except for IHC score analysis. Certain studies select a representative outcome from independent experiments for presentation, with independent experiments defined as those performed on separate days. No statistical method was used to predetermine sample size, and no data were excluded from the analyses. All data in the article and supplementary information are available.

Reagents used in this study are listed in Supplementary Table 1 and Supplementary Table 2.

Reporting summary

Further information on research design is available in the Nature Portfolio Reporting Summary linked to this article.

Data availability

Data from TCGA-COAD and TCGA-READ cohort used in this study were downloaded from Xena Browser[UCSC Xena]. The datasets including GSE18105, GSE44076, GSE87211, GSE103157 were downloaded from GEO database, PRJNA482620 was downloaded from NCBI BioProject[<https://www.ncbi.nlm.nih.gov/bioproject/PRJNA482620>], PHS000452 was downloaded from NCBI dbGaP[<https://www.ncbi.nlm.nih.gov/gap/?term=PHS000452>]. The raw data of RNA-seq generated in this paper was deposited in NCBI BioProject under the accession code PRJNA1183902, PRJNA1183903. The metabolomics data generated in this study have been deposited in the MetaboLights database under the accession code MTBLS11623. All data needed to support the conclusions in the paper are present in the paper or the Supplementary Materials. Source data are provided with this paper.

References

- Bray, F. et al. Global cancer statistics 2022: GLOBOCAN estimates of incidence and mortality worldwide for 36 cancers in 185 countries. *CA Cancer J. Clin.* **74**, 229–263 (2024).
- Li, Y. et al. Targeting MS4A4A on tumour-associated macrophages restores CD8+ T-cell-mediated antitumour immunity. *Gut* **72**, 2307–2320 (2023).
- Vilar, E. & Gruber, S. B. Microsatellite instability in colorectal cancer—the stable evidence. *Nat. Rev. Clin. Oncol.* **7**, 153–162 (2010).
- Goldstein, J. et al. Multicenter retrospective analysis of metastatic colorectal cancer (CRC) with high-level microsatellite instability (MSI-H). *Ann. Oncol.* **25**, 1032–1038 (2014).
- Kather, J. N., Halama, N. & Jaeger, D. Genomics and emerging biomarkers for immunotherapy of colorectal cancer. *Semin Cancer Biol.* **52**, 189–197 (2018).
- Locasale, J. W. Diet and exercise in cancer metabolism. *Cancer Discov.* **12**, 2249–2257 (2022).
- Martinez-Garay, C. & Djouder, N. Dietary interventions and precision nutrition in cancer therapy. *Trends Mol. Med.* **29**, 489–511 (2023).
- Bose, S., Allen, A. E. & Locasale, J. W. The molecular link from diet to cancer cell metabolism. *Mol. Cell* **78**, 1034–1044 (2020).
- Maddocks, O. et al. Modulating the therapeutic response of tumours to dietary serine and glycine starvation. *Nature* **544**, 372–376 (2017).
- Li, T. et al. Methionine deficiency facilitates antitumour immunity by altering m(6)A methylation of immune checkpoint transcripts. *Gut* **72**, 501–511 (2023).
- Gonzalez, P. S. et al. Mannose impairs tumour growth and enhances chemotherapy. *Nature* **563**, 719–723 (2018).
- Mackintosh, C. et al. Association of coffee intake with survival in patients with advanced or metastatic colorectal cancer. *JAMA Oncol.* **6**, 1713–1721 (2020).
- Oyelere, A. M. et al. Coffee consumption is associated with a reduced risk of colorectal cancer recurrence and all-cause mortality. *Int J. Cancer* **154**, 2054–2063 (2024).
- Guercio, B. J. et al. Coffee intake, recurrence, and mortality in Stage III colon cancer: results from CALGB 89803 (Alliance). *J. Clin. Oncol.* **33**, 3598–3607 (2015).
- Yoon, S., Lee, B. K. & Kim, K. P. Caffeine enhances chemosensitivity to irinotecan in the treatment of colorectal cancer. *Phytomedicine* **121**, 155120 (2023).
- Lopez-Barrera, D. M. et al. Spent coffee grounds, an innovative source of colonic fermentable compounds, inhibit inflammatory mediators in vitro. *Food Chem.* **212**, 282–290 (2016).
- Zhao, W. et al. Caffeine inhibits NLRP3 inflammasome activation by suppressing MAPK/NF- κ B and A2aR signaling in LPS-induced THP-1 macrophages. *Int. J. Biol. Sci.* **15**, 1571–1581 (2019).
- Tej, G., Neogi, K. & Nayak, P. K. Caffeine-enhanced anti-tumor activity of anti-PD1 monoclonal antibody. *Int. Immunopharmacol.* **77**, 106002 (2019).
- Darang, E. et al. Bioinformatics and pathway enrichment analysis identified hub genes and potential biomarker for gastric cancer prognosis. *Front. Oncol.* **13**, 1187521 (2023).
- Yan, Y. et al. COL12A1 as a prognostic biomarker links immunotherapy response in breast cancer. *Endocr. Relat. Cancer* **30**, e230012 (2023).
- Wu, Y. & Xu, Y. Integrated bioinformatics analysis of expression and gene regulation network of COL12A1 in colorectal cancer. *Cancer Med.* **9**, 4743–4755 (2020).
- Papanicolaou, M. et al. Temporal profiling of the breast tumour microenvironment reveals collagen XII as a driver of metastasis. *Nat. Commun.* **13**, 4587 (2022).
- Kenski, J. et al. An adverse tumor-protective effect of IDO1 inhibition. *Cell Rep. Med.* **4**, 100941 (2023).
- Li, H. et al. Indoleamine 2,3-dioxygenase mediates the therapeutic effects of adipose-derived stromal/stem cells in experimental periodontitis by modulating macrophages through the kynurenine-AhR-NRF2 pathway. *Mol. Metab.* **66**, 101617 (2022).
- Cheong, J. E. & Sun, L. Targeting the IDO1/TDO2-KYN-AhR Pathway for Cancer Immunotherapy - Challenges and Opportunities. *Trends Pharm. Sci.* **39**, 307–325 (2018).
- Rowland, B. D. & Peeper, D. S. KLF4, p21 and context-dependent opposing forces in cancer. *Nat. Rev. Cancer* **6**, 11–23 (2006).
- Tetreault, M. P., Yang, Y. & Katz, J. P. Kruppel-like factors in cancer. *Nat. Rev. Cancer* **13**, 701–713 (2013).
- Wang, X. et al. The deubiquitinase USP10 regulates KLF4 stability and suppresses lung tumorigenesis. *Cell Death Differ.* **30**, 2364 (2023).
- Ju, Y. et al. KLF4: a multifunctional nexus connecting tumor progression and immune regulation. *Front. Immunol.* **16**, 1514780 (2025).
- Nah, J. & Seong, R. H. Kruppel-like factor 4 regulates the cytolytic effector function of exhausted CD8 T cells. *Sci. Adv.* **8**, eadc9346 (2022).
- Li, X. et al. Navigating metabolic pathways to enhance antitumour immunity and immunotherapy. *Nat. Rev. Clin. Oncol.* **16**, 425–441 (2019).
- Proietti, E. et al. Polyamines and kynurenines at the intersection of immune modulation. *Trends Immunol.* **41**, 1037–1050 (2020).
- Xue, C. et al. Tryptophan metabolism in health and disease. *Cell Metab.* **35**, 1304–1326 (2023).
- Liu, Y. et al. Tumor-repopulating cells induce PD-1 Expression in CD8(+) T cells by transferring kynurenine and AhR Activation. *Cancer Cell* **33**, 480–494 (2018).
- Campesato, L. F. et al. Blockade of the AHR restricts a Treg-macrophage suppressive axis induced by L-Kynurenine. *Nat. Commun.* **11**, 4011 (2020).
- Triplett, T. A. et al. Reversal of indoleamine 2,3-dioxygenase-mediated cancer immune suppression by systemic kynurenine depletion with a therapeutic enzyme. *Nat. Biotechnol.* **36**, 758–764 (2018).
- Shi, M. et al. A novel KLF4/LDHA signaling pathway regulates aerobic glycolysis in and progression of pancreatic cancer. *Clin. Cancer Res.* **20**, 4370–4380 (2014).
- Han, Y. et al. Roles of KLF4 and AMPK in the inhibition of glycolysis by pulsatile shear stress in endothelial cells. *Proc. Natl Acad. Sci. USA* **118**, e2103982118 (2021).
- Liu, M. et al. Targeting the IDO1 pathway in cancer: from bench to bedside. *J. Hematol. Oncol.* **11**, 100 (2018).

40. Li, Y. et al. Increased coexpression of PD-L1 and IDO1 is associated with poor overall survival in patients with NK/T-cell lymphoma. *Leukemia* **38**, 1553–1563 (2024).
41. Foy, J. P. et al. The immune microenvironment of HPV-negative oral squamous cell carcinoma from never-smokers and never-drinkers patients suggests higher clinical benefit of IDO1 and PD1/PD-L1 blockade. *Ann. Oncol.* **28**, 1934–1941 (2017).
42. Xiang, Z. et al. A positive feedback between IDO1 metabolite and COL12A1 via MAPK pathway to promote gastric cancer metastasis. *J. Exp. Clin. Cancer Res.* **38**, 314 (2019).
43. Martin-Vega, A. & Cobb, M. H. Navigating the ERK1/2 MAPK Cascade. *Biomolecules* **13**, 1555 (2023).
44. Sanderson, S. M. et al. Methionine metabolism in health and cancer: a nexus of diet and precision medicine. *Nat. Rev. Cancer* **19**, 625–637 (2019).
45. Muthusamy, T. et al. Serine restriction alters sphingolipid diversity to constrain tumour growth. *Nature* **586**, 790–795 (2020).
46. Locasale, J. W. Serine, glycine and one-carbon units: cancer metabolism in full circle. *Nat. Rev. Cancer* **13**, 572–583 (2013).
47. Taylor, S. R. et al. Developing dietary interventions as therapy for cancer. *Nat. Rev. Cancer* **22**, 452–466 (2022).
48. Prendeville, H. & Lynch, L. Diet, lipids, and antitumor immunity. *Cell Mol. Immunol.* **19**, 432–444 (2022).
49. Fan, Y. et al. Effects of diets on risks of cancer and the mediating role of metabolites. *Nat. Commun.* **15**, 5903 (2024).
50. Lee, S. M. et al. Aryl hydrocarbon receptor – targeted therapy for CD41 Tcell – mediated idiopathic pneumonia syndrome in mice. *Blood* **139**, 3325–3339 (2022).
51. Lee, S. M. et al. Inhibition of acute lethal pulmonary inflammation by the IDO – AhR pathway. *Proc. Natl Acad. Sci. USA*. **114**, E5881–E5890 (2017).
52. Lan, Y. et al. Effect of radiation fractionation on IDO1 via the NF- κ B/COX2 axis in non-small cell lung cancer. *Int Immunopharmacol.* **124**, 110956 (2023).

Acknowledgements

This study was supported by grants from the National Natural Science Foundation of China (81972631, 82273039, 82472887 awarded to H.D., 82103595 awarded to Y.F., 82073063 awarded to Z.S.); The Guangdong Provincial Key Laboratory of Precision Medicine for Gastrointestinal Cancer (2020B121201004 awarded to H.D.); The Natural Science Foundation of Guangdong Province (2021A1515010989 awarded to H.D., 2022A1515010298 awarded to Z.S., 2022A1515111142 awarded to Y.Z.); Guangdong Basic and Applied Basic Research Foundation, China (2023A1515010274 awarded to H.D., 2023A1515011789, 2025A1515011911 awarded to Y.F., 2023A1515010980 awarded to Z.S.); Guangdong Provincial Regional Joint Fund-Youth Fund Project (2020A151110006 awarded to Y.F.); Guangzhou Key Research and Development Project (202206080008 awarded to H.D.); Outstanding Youth Development Scheme of Nanfang Hospital, Southern Medical University (2020J010 awarded to Z.S.).

We thank all laboratory members of the Department of Pathology of Southern Medical University for their support and comments. And we

thank UK Biobank for their data support. The schematic diagram of the graphical abstract, the images of mice elements and co-culture were drawn by [Figdraw.com](https://figdraw.com).

Author contributions

YC.L., Y.F. and H.D. designed the study. YC.L. and Z.L. carried out most of the experiments and drafted the manuscript. Y.H., YY.L. and Y.Z. performed the animal breeding and made statistical analyses. S.Q. and Y.L. discussed the data and drew the diagrams. H.D. and Z.S. supervised the study. (YC.L., Yuechen Liu; YY.L., Yunyan Ling, Y.L., Yang Liu). Y.F. analyzed the UK Biobank data. All authors reviewed and approved the manuscript.

Competing interests

The authors declare no competing interests.

Additional information

Supplementary information The online version contains supplementary material available at <https://doi.org/10.1038/s41467-025-60958-0>.

Correspondence and requests for materials should be addressed to Zhiyong Shen, Yuan Fang or Haijun Deng.

Peer review information *Nature Communications* thanks Luisa Lopes, and the other, anonymous, reviewer(s) for their contribution to the peer review of this work. A peer review file is available.

Reprints and permissions information is available at <http://www.nature.com/reprints>

Publisher's note Springer Nature remains neutral with regard to jurisdictional claims in published maps and institutional affiliations.

Open Access This article is licensed under a Creative Commons Attribution-NonCommercial-NoDerivatives 4.0 International License, which permits any non-commercial use, sharing, distribution and reproduction in any medium or format, as long as you give appropriate credit to the original author(s) and the source, provide a link to the Creative Commons licence, and indicate if you modified the licensed material. You do not have permission under this licence to share adapted material derived from this article or parts of it. The images or other third party material in this article are included in the article's Creative Commons licence, unless indicated otherwise in a credit line to the material. If material is not included in the article's Creative Commons licence and your intended use is not permitted by statutory regulation or exceeds the permitted use, you will need to obtain permission directly from the copyright holder. To view a copy of this licence, visit <http://creativecommons.org/licenses/by-nc-nd/4.0/>.

© The Author(s) 2025